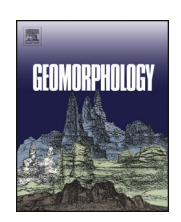
ELSEVIER

Contents lists available at ScienceDirect

Geomorphology

journal homepage: www.elsevier.com/locate/geomorph



Foredune morphodynamics and sediment budgets at seasonal to decadal scales: Humboldt Bay National Wildlife Refuge, California, USA



Alana M. Rader ^a, Andrea J. Pickart ^b, Ian J. Walker ^{c,*}, Patrick A. Hesp ^d, Bernard O. Bauer ^e

- ^a Department of Geography, School of Arts and Sciences, Rutgers University, 54 Joyce Kilmer Ave., Piscataway, NJ 08854, USA
- ^b U.S. Fish and Wildlife Service, Humboldt Bay National Wildlife Refuge, 6800 Lanphere Rd., Arcata, CA 95521, USA
- School of Geographical Sciences & Urban Planning, School of Earth & Space Exploration, Arizona State University, P.O. Box 875302, Tempe, AZ 85287-5302, USA
- d Beach and Dune Systems Laboratory (BEADS), Faculty of Science and Engineering, Flinders University, GPO Box 2100, Adelaide 5001, South Australia, Australia
- e Earth, Environmental and Geographic Sciences, Irving K. Barber School of Arts and Sciences, University of British Columbia, Okanagan 1177 Research Road, Kelowna, BC VIV 1V7, Canada

ARTICLE INFO

Article history: Received 18 September 2017 Received in revised form 27 May 2018 Accepted 4 June 2018 Available online 8 June 2018

Keywords: Foredune Aeolian Coastal erosion Shoreline change

ABSTRACT

Coastal foredunes are shore-parallel ridges that form in the backshore and their morphodynamics are controlled partly by seasonal and spatial variations in the coastal (onshore) sediment budget that, in turn, are driven by oceanic and atmospheric processes and interactions, including regional wave and wind regimes, climatic variability events (e.g., ENSO), sediment availability, beach characteristics (e.g., width, slope), and vegetation type and cover in the backshore. Previous studies on shoreline change in Northern California report only broad rates of erosion and accretion related to regional meteorological regimes. This study presents a more detailed, multi-decadal to seasonal account of shoreline response and foredune morphodynamics along a 2.5 km stretch of coast in the Humboldt Bay National Wildlife Refuge (HBNWR). Analysis of historical aerial photography (1939–2014) reveals trends in shoreline position that are coupled with more detailed assessments of foredune morphodynamics and seasonal scale volumetric changes from cross-shore topographic profiles. These findings set the historical context of foredune morphodynamics and allow exploration of the implications of seasonal meteorological variation on long-term (75-year) foredune evolution and development at the HBNWR.

DSAS describes maximum foredune progradation in the north (up to $+0.51 \, \mathrm{m \, a^{-1}}$) and maximum foredune retreat in the south (up to $-0.49 \, \mathrm{m \, a^{-1}}$). Aerial photograph analysis (2004–2014) shows statistically significant larger erosive features in the southern zone than in the northern and central zones. Seasonal volume calculations from cross-shore profiles indicate statistically significant differences in alongshore transect elevation and foredune volume, with larger elevations and volumes in the northern and central zones than in the southern. Combined with evidence of seasonal bidirectional littoral drift, these data support a north to south gradient in sediment availability, foredune position and resulting stages of established foredune development. Seasonal storm energies and climate forcing events introduce variability in erosive patterns but support the persistence of alongshore developmental stages. Future research should explore foredune morphodynamics on a smaller spatial scale and changes related to the presence/absence of multiple vegetation assemblages.

© 2018 Published by Elsevier B.V.

1. Introduction

Coastal foredunes evolve as a consequence of aeolian sediment transport across the beach and subsequent deposition on the backshore in the presence of roughness elements such as vegetation, wrack, and wood debris (Godfrey, 1977; Goldsmith, 1989; Hesp, 1989; Hemming and Nieuwenhuize, 1990; Arens, 1996; Hesp, 2002; Eamer and Walker, 2010; Luna et al., 2011). Incipient foredunes often develop as

shore-parallel ridges that evolve via sedimentation within pioneer plant communities and backshore debris (Hesp, 1984, 2002; Arens and Wiersma, 1994; Eamer and Walker, 2010; Luna et al., 2011; Nordstrom et al., 2011a, b). Under stable coastline conditions, and with sustained sand delivery to the backshore, incipient dunes may grow and become established foredunes, characterized by morphological complexity and late-stage successional plant communities (Hesp, 1988a, b, 2002; Pickart and Sawyer, 1998; Heathfield and Walker, 2011). Deposition patterns on foredunes are thus widely dependent on the spatial zonation, density, distribution, and physical characteristics of dune plant species (Hesp, 1988a, b; Arens, 1996; Ruggiero et al., 2011). Open sand surface areas and increased exposure to aeolian action are greatest during winter months on some coasts and in latitudes north of 40° (Davidson-Arnott and Law, 1996; Davidson-Arnott,

^{*} Corresponding author at: School of Geographical Sciences & Urban Planning, School of Earth & Space Exploration, Arizona State University, P.O. Box 875302, Tempe, AZ, USA. E-mail addresses: arader@uvic.ca (A.M. Rader), andrea_pickart@fws.gov (A.J. Pickart), ianjwalker@asu.edu (I.J. Walker), patrick.hesp@flinders.edu.au (P.A. Hesp), bernard.bauer@ubc.ca (B.O. Bauer).

2010 - see his figure 9.23), whereas increased vegetation cover, surface sheltering, and aeolian deposition within the plant canopy prevail during the summer growth season. Such phenological controls are most pronounced in areas where vegetation dies back to a point where it is unable to recover to its previous extent. The absence of vegetation may lead to an increase in wave erosion in the winter coupled with pronounced aeolian transport of drier sediments across foredunes during the summer (Goldsmith, 1989; Arens, 1996; Hesp, 2002; Kuriyama et al., 2005; Walker et al., 2017).

Foredune morphodynamics, or changes in morpho-ecological states of coastal dunes, are a function of local ecology as well as adjacent beach-surfzone processes, such as wind energy, wave energy and type, sediment supply, and littoral drift direction (Short and Hesp, 1982; Hesp, 1988a, b, 2002; Sherman and Bauer, 1993; Scott et al., 2010; Ollerhead et al., 2013; Houser and Ellis, 2013; Walker et al., 2017). These factors influence sediment transport and delivery patterns within and between major geomorphic components (i.e., the beach, foredune and backdunes) of the beach-dune system, ultimately controlling dune form, recovery from erosive events, and longer-term shoreline positions (e.g., Bauer and Davidson-Arnott, 2002; Miot da Silva and Hesp, 2010; Delgado-Fernandez and Davidson-Arnott, 2009, 2011; Houser and Ellis, 2013; Hesp and Smyth, 2016). Additional extreme forcing from dynamic wind, wave and water level regimes associated with seasonal storms or climatic variability may also alter littoral and aeolian sediment transport exchanges between morphological components. For example, previous research in the Pacific Northwest has linked occurrences of El Niño Southern Oscillation (ENSO) phases to increased mean water level, increased significant wave height, and shifts in dominant wave direction (Ruggiero et al., 2001; Subbotina et al., 2001; Allan and Komar, 2002; Barnard et al., 2015). Changes in these conditions with ENSO phases can, in turn, alter the local sediment budget response of shorelines as has been observed across the Pacific Ocean basin (Storlazzi et al., 2000; Allan and Komar, 2002; Heathfield et al., 2013; Barnard et al., 2015). As such, a sediment budget (volumetric change) approach can be used to provide insight into the links between key morphological responses within beach-dune ecosystems, broader regional forcing signals, and the resultant morphological evolution of the foredune.

Previous studies have shown that beach-foredune sediment budgets can be easily quantified at the meso-scale (with a spatial extent of 10s of metres to kilometres and an annual to decadal temporal scale) (Davidson-Arnott and Law, 1996; Darke et al., 2016). Despite this, there are relatively few meso-scale studies of beach-dune sediment transport repeated frequently enough to capture seasonal controls on foredune morphodynamics (e.g., McLean and Thom, 1975; Anthony et al., 2006; Delgado-Fernandez and Davidson-Arnott, 2009; Arens et al., 2013; Hesp, 2013; Ollerhead et al., 2013; Walker et al., in press). Repeated morphological monitoring using cross-shore transects (e.g., McLean and Thom, 1975; Ollerhead et al., 2013) or detailed land surveys (e.g., Darke et al., 2013; Eamer and Walker, 2013) allow for observation of erosion and deposition and related volumetric changes. In turn, these observations can be quantified to estimate seasonal volume change and/or foredune development in coastal dune ecosystems.

The purpose of this paper is to examine and quantify historical changes in foredune morphology and position in relation to beachforedune sediment budgets at the Humboldt Bay National Wildlife Refuge (HBNWR) in Northern California. Dunes at this site have been the focus of several coastal management projects, beginning with small-scale invasive species management in the 1980s, complete removal of invasive *Ammophila arenaria* within a particular dune units in the late 1990s and early 2000s, and more recent follow up vegetation treatments (further information in Pickart, 2013, 2014). During these projects, various datasets were generated from which morphological changes can be assessed, predominantly from aerial photographs and, cross-shore topographic survey transects. The monitoring history at

this site provides a unique opportunity to quantify meso-scale sediment budget patterns and foredune morphodynamics. The specific research objectives of this study are to analyse and interpret interannual to decadal scale changes in coastal dune morphology and shoreline positions from aerial photography between 1939 and 2014. In addition, the study examines recent seasonal variability in erosion and accretion patterns in the beach-dune system and discusses implications for the long-term evolution of the foredune complex.

2. Study site

This study was conducted in the Lanphere and Ma-le'l coastal dune systems within HBNWR located near Arcata in Northern California. The study area consisted of a 2.5 km stretch of established foredunes to the north of Humboldt Bay and the Eel River and south of the Little and Mad Rivers (Fig. 1). Transport of discharged sediment from streams is a dominant source of sediment for California beaches (Willis and Griggs, 2003; Wheatcroft and Sommerfield, 2005; Patsch and Griggs, 2006). Average annual sand and gravel discharge for the Little, Mad and Eel Rivers is estimated at 40,680 m³ a⁻¹, 525,509 m³ a⁻¹, and 2,869,455 m³ a⁻¹, respectively, although exact contribution to the overall littoral sediment budget remains unknown (Willis and Griggs, 2003) and Eel River discharge measurement errors may have exaggerated its contribution by a factor of 2.5 (Warrick, 2014).

The site was divided into northern, central and southern zones according to dominant long-term (1939-2014) trends in foredune position (Fig. 1). The established foredunes at the study site are continuous alongshore and often fronted by incipient foredunes that vary in size and persistence over time, depending on wind and wave run-up patterns, storm frequency, beach widths, and the presence or absence of pioneer plant communities. The foredunes are backed by active parabolic and transgressive dune fields and deflation basins. The dunes are oriented toward the SE, in alignment with formative onshore winds from the NNW during late spring through summer (April-September). The resultant drift direction is 128.7° for aeolian sediment transport based on estimation of regional transport using the model of Fryberger and Dean (1979) (Fig. 2). Dominant offshore winds come from the SE in the fall and winter months (October-March), with about 12% and 13% of cumulative winds coming from the SE and S. respectively. A sediment transport threshold of 6.76 m s⁻¹ was calculated using the Bagnold (1941) model and the average grain size of samples collected at the site ($D_{50} = 0.23$ mm).

Dominant wave direction varies seasonally, coming from the NNW from April to September and predominantly from the WNW from October to March (Fig. 3). Furthermore, taller, longer period waves occur in the fall-winter, compared to the more frequent shorter wave heights from April to September (Fig. 3). Seasonal shifts in wind and wave regimes lead to bi-directional longshore drift for the Eureka Littoral Cell (Dingler and Clifton, 1994; Hapke et al., 2006, 2009). For example, wind and wave directions from the NW combine with sediment supply from the Little and Mad Rivers to drive a net southerly longshore drift direction during the summer months (Figs. 1, 2). During the winter season, from October to March, dominant offshore wind directions from the SE and wave directions out of the WNW align with a seasonal southward and offshore shift in the Hawaiian High Pressure system. These meteorological conditions contribute to a net (but variable) littoral drift direction from the south to the north (relative to the orientation of the shoreline, which is oriented slightly NE-SW) (Hapke et al., 2006, 2009). An increase in storm-generated North Pacific swell reaching the coast, normally having the capacity to bring sediment onshore, may instead cause localized erosion if offshore sediment supply is limited. For example, erosion at the southern portion of the study site from winter storm waves may occur as net northerly waves deposit transported offshore sediment from the Eel River when contacting the Humboldt Bay Jetty system.

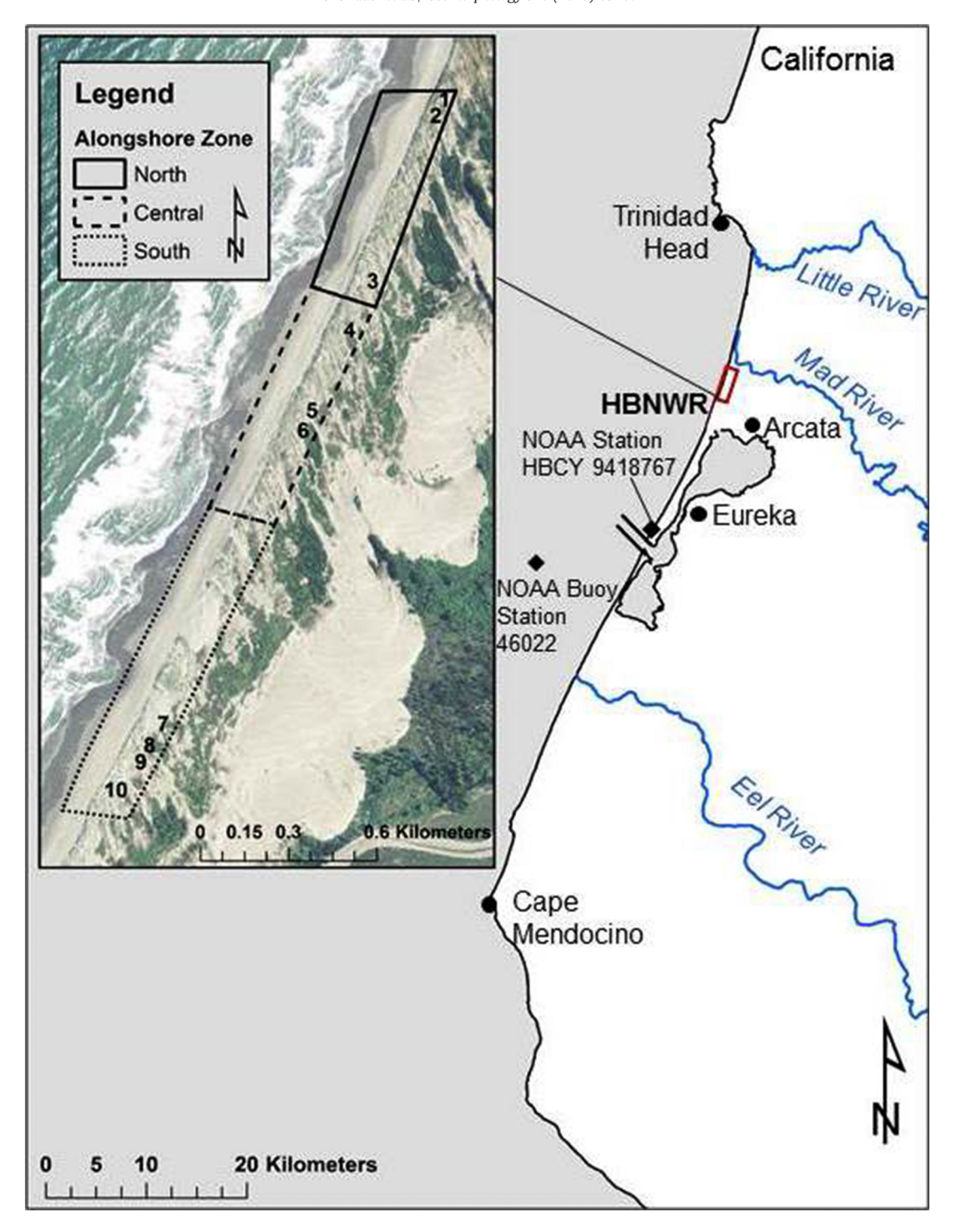


Fig. 1. Regional map of (HBNWR) near Arcata and Eureka in Northern California, USA. Inset photo shows northern, central and southern alongshore zones. Coincident topographic survey locations are also indicated. Cross shore transects from topographic surveys are oriented to the NW, in the direction of dominant transporting wind directions and the transgressive dune system.

3. Methods

3.1. Meteorological data and analysis

Wind speed and direction data for 2015 were collected from 24-hour observations for North Spit, CA (Data source: Station HBYC1, 94187667). These data were used to produce annual and seasonal wind roses and frequency tables for the 16 cardinal directions using Lakes Environmental WRPlot View software. Mean grain size of surface

sediment samples was calculated using GRADISTAT version 8 (Blott and Pye, 2001) and used to calculate a sediment transport threshold using the Bagnold (1941). model. Finally, an aeolian sediment drift rose was produced using the Fryberger and Dean (1979) model and m s⁻¹ transport threshold per methods outlined in Miot da Silva and Hesp (2010).

Seasonal storm events typically generate elevated storm surges, wave heights and wave run-up causing potential erosion and landward shoreline retreat when water surge exceeds a mean high high water level (MHHWL) (Allan and Komar, 2002; Allan et al., 2003). For this

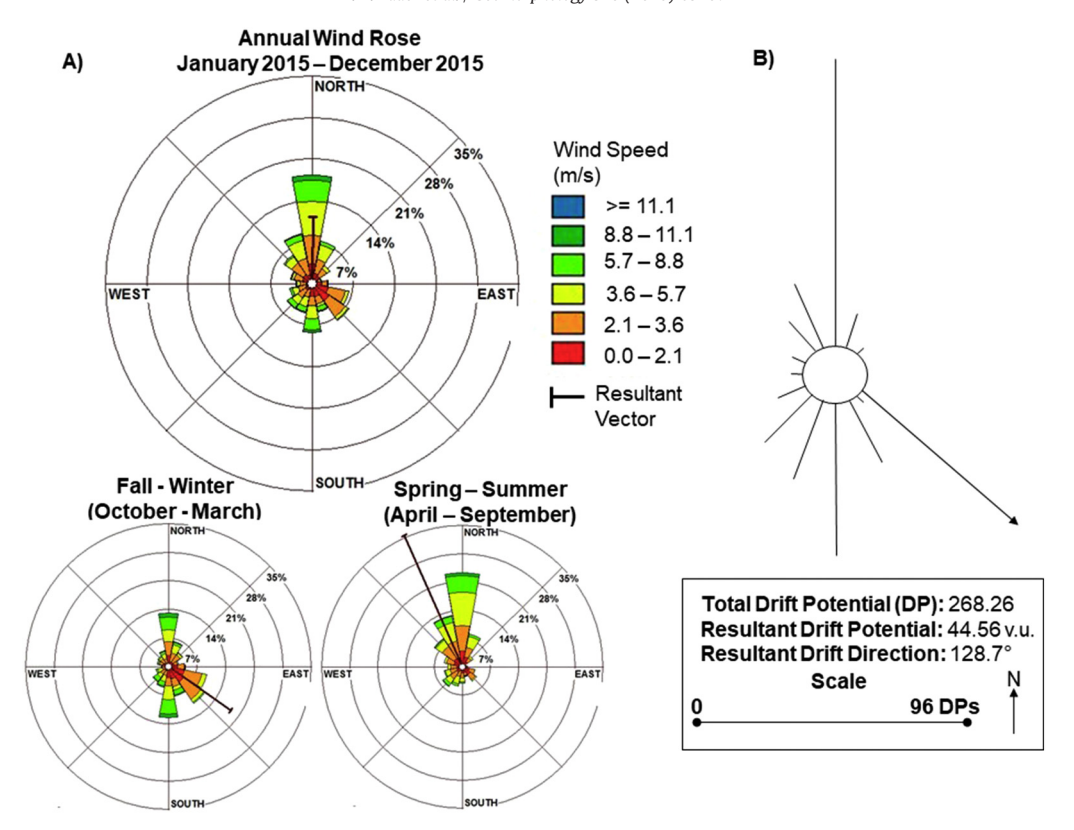


Fig. 2. Annual wind rose (A) and aeolian sediment drift potential rose (B) generated from 24-hour observations for 2015 for North Spit, CA. Resultant wind vectors show average wind direction. The sediment drift potential rose shows drift potential (DP) from almost all compass directions and the resultant drift direction vector (RDD, black arrow length in vector units) toward the SSE. The wind rose was generated using Lakes Environmental's WR Plot (https://www.weblakes.com/products/wrplot) while the aeolian sediment drift rose was produced using the Fryberger and Dean (1979) method with m s⁻¹ wind data per Miot da Silva and Hesp (2010). (Data source: Station HBYC1, 94187667 at North Spit, CA). Overall direction of resultant wind vector is 1°, while fall-winter and spring-summer intervals see resultant vector directions of 125° and 336°, respectively.

study, the seaward toe of the established foredune was identified from a light detection and ranging (LiDAR) derived bare earth model from May 2015. The line delineating the foredune toe represents a threshold above which the established foredune can be eroded by wave action. The foredune toe line was digitized in QT Modeler software version 8. As the exact position and resulting elevation of the foredune toe varies alongshore with spatially varying impacts of surf zone-beach processes (Hesp, 1988a, b), elevation values from the digitized foredune toe were averaged across the study site and used as a single proxy for the erosional threshold of the foredune.

Variability in sea level and wave dynamics occur during phases of climate forcing phenomena. Recent research has shown a link between positive phases of monthly to interannual ENSO phases (El Niño) and multiyear to decadal Pacific Decadal Oscillation (PDO) events to increased frequency of extreme storms on the west coast of North America (Abeysirigunawarbena and Walker, 2008; Abeysirigunawarbena et al., 2009). For example, El Niño and PDO are both characterized by warmer sea surface temperatures in the coastal northeastern Pacific and localized variability in precipitation and wind regimes (Wolter and Timlin, 1998; Storlazzi and Wingfield, 2005; Barnard et al., 2015). Average monthly values of three main climate indices commonly used to quantify phases of climate variability and ocean-atmosphere anomalies were collected from NOAA Earth System Research Laboratory for the period 1982-2012. Positive values of the Multivariate ENSO Index (MEI) and the Pacific Decadal Oscillation (PDO) are associated with conditions characteristic of warm ENSO (El Niño) and PDO phases respectively, such as warmer sea surface temperatures and increased water levels along the west coast of North America. Negative values of the MEI and PDO indices are associated with conditions characteristic of cold ENSO phases (La Niña), in which lower sea surface temperatures and increased upwelling in the eastern Pacific have been observed. The Northern Oscillation Index (NOI) is a regionally defined index that describes positive and negative ENSO phases according to variations in sea-level pressure in the Northeast Pacific and Darwin, Australia (Schwing et al., 2002). NOI values, in contrast to the MEI and PDO indices, associates positive NOI values with La Niña and negative NOI values with El Niño. Climate variability index values were plotted against corresponding water level and wave height data to isolate periods of increased localized energy that may be associated with climate forcing phenomena.

3.2. Aerial photographic analyses

Aerial photographs from 1939 to 2014 with sufficient coverage of the study site (i.e., seaward extent of vegetation visible, all transect locations visible) and relatively large scales (i.e., 1:25,000 or greater) were analysed to detect changes in foredune morphology and position (Table 2). To minimize bias introduced from aerial photographs of varying quality, extra care was taken to normalize image resolutions. For example, low resolution or high contrast images can affect digitization precision, in turn skewing interpretation of dune position change analysis. As such, aerial photographs were resampled within ArcGIS software to represent the lowest pixel resolutions of 1 m. A bi-linear interpolation method was chosen to resample aerial photographs because the original continuous pixel values can be retained in the new resampled image. Resampled aerial photographs from 1939 through 1992 were georeferenced to the rectified USDA-NAIP 2014 photograph using 10 identical ground control points (GCP) identified from the corner of physical structures (e.g., houses, airports) and road intersections. The photos were orthorectified in QGIS using the UTM Zone 10 coordinate system and the 1983 North American Datum (NAD83). A nearest neighbour resampling method and Polynomial 1 transformation type were used to transform the georeferenced aerial photographs to the

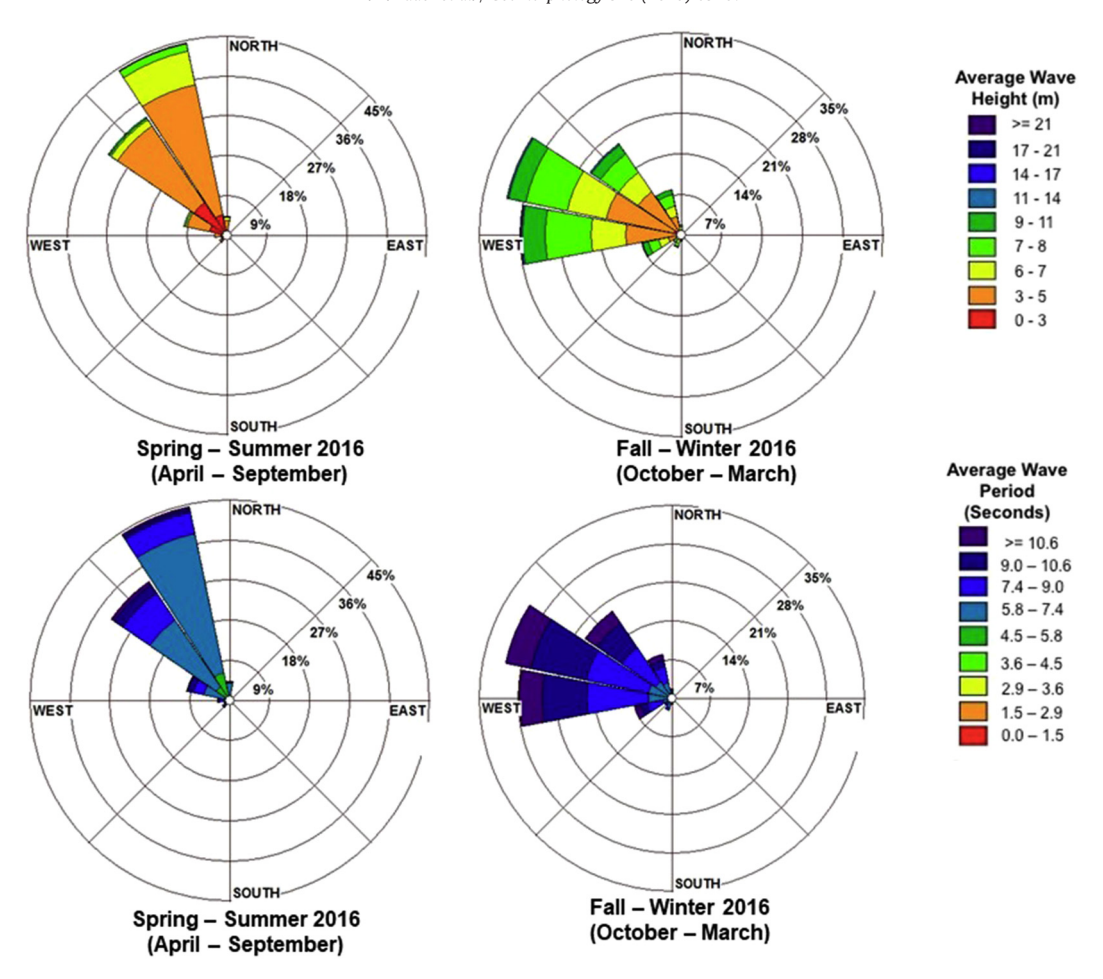


Fig. 3. Annual wave roses generated from 24-hour observations of significant wave height (m), average wave period (seconds) and wave direction (degrees) in 2016 at the NOAA Buoy Station 46,022 at Eel River, CA. Wave roses were generated using Lakes Environmental's WR Plot (https://www.weblakes.com/products/wrplot). Resultant vector data describes spring-summer waves coming from 316°, and from 289° in the fall-winter interval.

coordinates of the 2014 NAIP imagery (Thieler and Danforth, 1994). The resulting orthorectified aerial photographs, along with the USDA-NAIP digital aerial photograph series, were used as a reference for the digitization of the seaward extent of vegetation and other relevant geomorphic units.

Georeferencing error was accounted for using the root-mean-square error (RMSE) method as per Wang et al. (2012) when assessing accuracy of the polynomial least squares geometric correction. RMSE values

Table 1

Annual significant wave height (m), average wave period (s) and long-term monthly water level (m) for the period 1980 to 2014. Annual maxima and minima are listed in brackets. Wave data recorded at NOAA Buoy Station 46022 at Eel River, CA. (Data acquired: March 14, 2017 from http://www.ndbc.noaa.gov/station_history.php?station=46022). Long term (1980–2014) average monthly water level data recorded from NOAA Tidal Station 9418767 (Date acquired: March 28, 2017. Data source: https://tidesandcurrents.noaa.gov/datums.html?units=1&epoch=0&id=9418767&name=North+Spit&state=CA).

| | Annual | Fall-Winter (November-March) | Spring-Summer (April-October) |
|--|-----------------------|---------------------------------|----------------------------------|
| Hourly average significant wave height (m) | 2.53 (10.79, 0.01) | 2.96 | 2.01 |
| Hourly average wave period (s) | 7.32 (16.81, 2.55) | 8.09 | 6.77 |
| Monthly mean water level (m) | 5.57 (7.45, 3.55) | 5.62 | 5.53 |

Table 2Date, source, original format and resampling information of 75-year aerial photograph record for geomorphic mapping and shoreline change analyses.

| Aerial | photographs | | | | | |
|---------|-------------------------|--|--|--|--|--|
| Resam | pling parameters: | | | | | |
| 1 m re | solution | Bilinear interpolation | | | | |
| Origin | al format: | Used for: | | | | |
| Scann | ed GeoTIFFs | - Long-term foredune position change | | | | |
| | | - Decadal-scale foredune position change | | | | |
| Date | Original resolution (m) | Source | | | | |
| 1939 | 0.29 | Humboldt County Public Works | | | | |
| 1948 | 0.70 | Historic Atlas of Humboldt Bay and Eel River Delta | | | | |
| 1954 | 0.75 | As above | | | | |
| 1958 | 0.50 | As above | | | | |
| 1965 | 0.70 | As above | | | | |
| 1981 | 1.00 | As above | | | | |
| 1992 | 1.00 | As above | | | | |
| Origin | al format: | Used for: | | | | |
| Digital | lorthophotographs | - Geomorphic mapping | | | | |
| | | - Long-term foredune position change | | | | |
| | | - Decadal-scale foredune position change | | | | |
| Date | Original resolution (m) | Source | | | | |
| 2004 | 1.00 | USDA National Agriculture Imagery Program (NAIP) | | | | |
| 2005 | 1.00 | As above | | | | |
| 2007 | | As above | | | | |
| 2009 | 1.00 | As above | | | | |
| 2010 | 1.00 | As above | | | | |
| 2012 | 1.00 | As above | | | | |
| 2014 | 1.00 | As above | | | | |

Table 3Georeferencing error (Wang et al., 2012) and digitization error (Thieler and Danforth, 1994) calculated for aerial photographs from 1939 to 2014. DSAS derived end point rate (EPR) error is calculated for each study interval using methods outlined by Thieler and Danforth (1994).

| Method error (I | erencing er d used: roo RMSE) of g ocation res | t mean squ round con | | Digitization error (m) Method used: average DSAS shoreline change envelope (SCE) statistic | | | |
|--------------------|---|-------------------------|-----------------------|--|-----------------------------------|---|--|
| Date | RMSE (m) | SCE (m) | Total error (m) | EPR intervals | Average of total errors (m) | DSAS EPR error (m a ⁻¹) | |
| 1939 | 10.15 | 7.07 | 17.23 | 1939-1948 | 18.10 | 2.01 | |
| 1948 | 6.50 | 12.47 | 18.97 | 1948-1954 | 16.07 | 2.68 | |
| 1954 | 5.02 | 8.15 | 13.18 | 1954-1958 | 14.23 | 3.56 | |
| 1958 | 7.12 | 8.16 | 15.28 | 1958-1965 | 13.32 | 1.90 | |
| 1965 | 6.05 | 5.32 | 11.37 | 1965-1981 | 13.26 | 0.83 | |
| 1981 | 5.01 | 10.14 | 15.16 | 1981-1992 | 9.69 | 0.88 | |
| 1992 | 2.23 | 2.00 | 4.23 | 1992-2004 | 4.04 | 0.34 | |
| 2004 | 0.15 | 3.71 | 3.86 | 2004-2005 | 3.19 | 3.19 | |
| 2005 | 0.15 | 2.36 | 2.51 | 2005-2009 | 3.27 | 0.82 | |
| 2009 | 0.15 | 4.18 | 4.33 | 2009-2010 | 3.73 | 3.73 | |
| 2010 | 0.15 | 3.28 | 3.43 | 2010-2012 | 3.16 | 1.58 | |
| 2012 | 0.15 | 3.04 | 3.19 | 2012-2014 | 3.62 | 1.81 | |
| 2014 | 0.15 | 4.20 | 4.35 | 1939-2014 | 9.01 | 0.12 | |

were calculated for each georeferenced (1939–1992) aerial photograph using the residual x and y positional uncertainty values for the 10 GCPs in each photograph (Table 3). Industry standard accuracy values of 0.15 m were assigned for each photograph within the UDSA NAIP digital aerial photograph series (2004–2014) (Table 3).

3.3. Foredune position change analysis

Foredune position changes were quantified using the Digital Shoreline Analysis System (DSAS) developed by the United States Geological Survey (Thieler et al., 2009), which operates as a plugin for ArcGIS version 10. DSAS statistics are generated from the measurement of multiple digitized historical 'shorelines' in reference to a static user-defined baseline. For this study, a fixed baseline was established at the landward origin of ten topographic sampling transects. 'Shoreline' shapefiles were digitized using the seaward-most line of established foredune vegetation, excluding the incipient foredune. The incipient foredune was excluded due to inconsistencies in the ability to delineate sparse pioneer plant communities within the backshore. The resulting line shapefile is considered a proxy for the seaward toe of the established foredune (Fig. 4). Location of cross shore transects was generated by DSAS at 5 m intervals alongshore for a detailed representation of calculated foredune toe positions at an equivalent spatial scale of observed geomorphic units. DSAS-derived end point rate (EPR), or rate of annual foredune position change, were calculated in m a⁻¹ by dividing the total distance of foredune toe movement by the number of years between the oldest and youngest shoreline shapefile as captured in the photos. EPR statistics were used to explore both the long-term average positional change of the foredune (1939–2014) and decadal-scale patterns of foredune change (i.e., 1939–1948, 1948–1954, 1954–1958, etc.) (Table 3).

DSAS error thresholds contain positional uncertainty (i.e., georeferencing RMSE) and measurement (digitization) uncertainty (Thieler and Danforth, 1994). The DSAS shoreline change envelope (SCE) was used to calculate digitization error for each photo year as suggested by Thieler and Danforth (1994) (Table 3). SCE represents the distance between shoreline shapefiles measured farthest from and closest to a defined baseline for each DSAS generated transect. Three shoreline shapefiles for each photo year were digitized from the visible seaward-most vegetation line by the same operator (Fig. 4). The resulting duplicate shapefiles were input into DSAS to produce SCE statistics for their respective photo years. The total error was calculated for each photo by adding corresponding georeferencing and digitization error values (Table 3). Finally, following Thieler and Danforth (1994), EPR errors were calculated for each DSAS interval by dividing the average of the total error values of all aerial photographs included in each study interval by the number of years between the first and last photograph in each series (Table 3). The resulting error represents a detection threshold value for annual foredune position change (in m a^{-1}), below which change is considered undetectable, or within the margins of error.

3.4. Geomorphic mapping

Aerial photographs from 2004 to 2014 were used to identify and digitize changes in topography using ArcGIS. The high resolution and colorized format of this photo series allowed for accurate identification of erosional and depositional units, partly through the visual presence/absence of vegetation. Additionally, the consistent timing of NAIP imagery, acquired annually during the local growing season, reduced

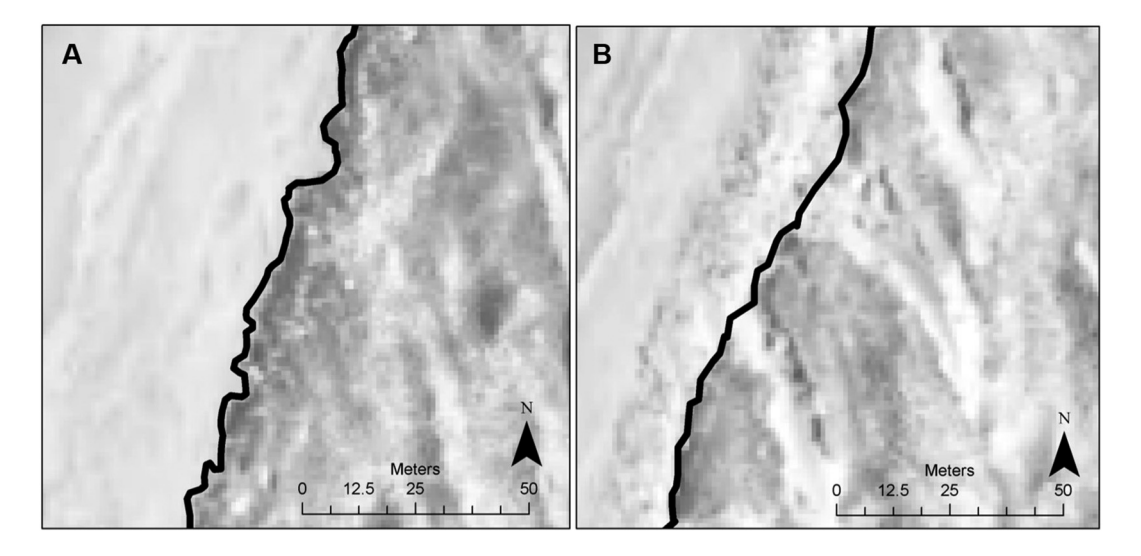


Fig. 4. The identification of the visible vegetation line on the established foredune and its resultant digitization of as a proxy for the foredune toe position, which was used to create a 'shoreline' from the 2012 USDA-NAIP aerial photograph using DSAS. A) Digitized shoreline shapefile in a simple delineation of the visible vegetation line with no incipient foredune zone while B) shows complex delineation of the visible vegetation line where incipient foredune zones and blowouts are also observed seawards of this line.

potential image interpretation bias associated with phenology and seasonal storms. Although small differences in timing may introduce inconsistencies (e.g., sun angle, atmospheric variability) in feature identification and image quality, previous studies have found that errors from these timing differences are acceptable for environmental management and research (Davies et al., 2010). Polygons delineating unvegetated deflation basins, extending from the visible vegetation line, past the crest, and into the backdune, were used as a proxy for erosional units following research on blowout identification in coastal

dunes (Jungerius and van der Meulen, 1989; Andrews et al., 2002). Depositional unit polygons were digitized from visible pioneer plant communities on the upper beach, seaward of the toe of established foredunes (Fig. 5). Geomorphic units were grouped into northern, central and southern units, as defined by alongshore zones distinguished by different rates of change in foredune position (Fig. 1). The total surface area of erosional and depositional units was calculated in ArcGIS and normalized by dividing the total erosional unit and incipient foredune areas in the northern, central and southern zone by the total area of

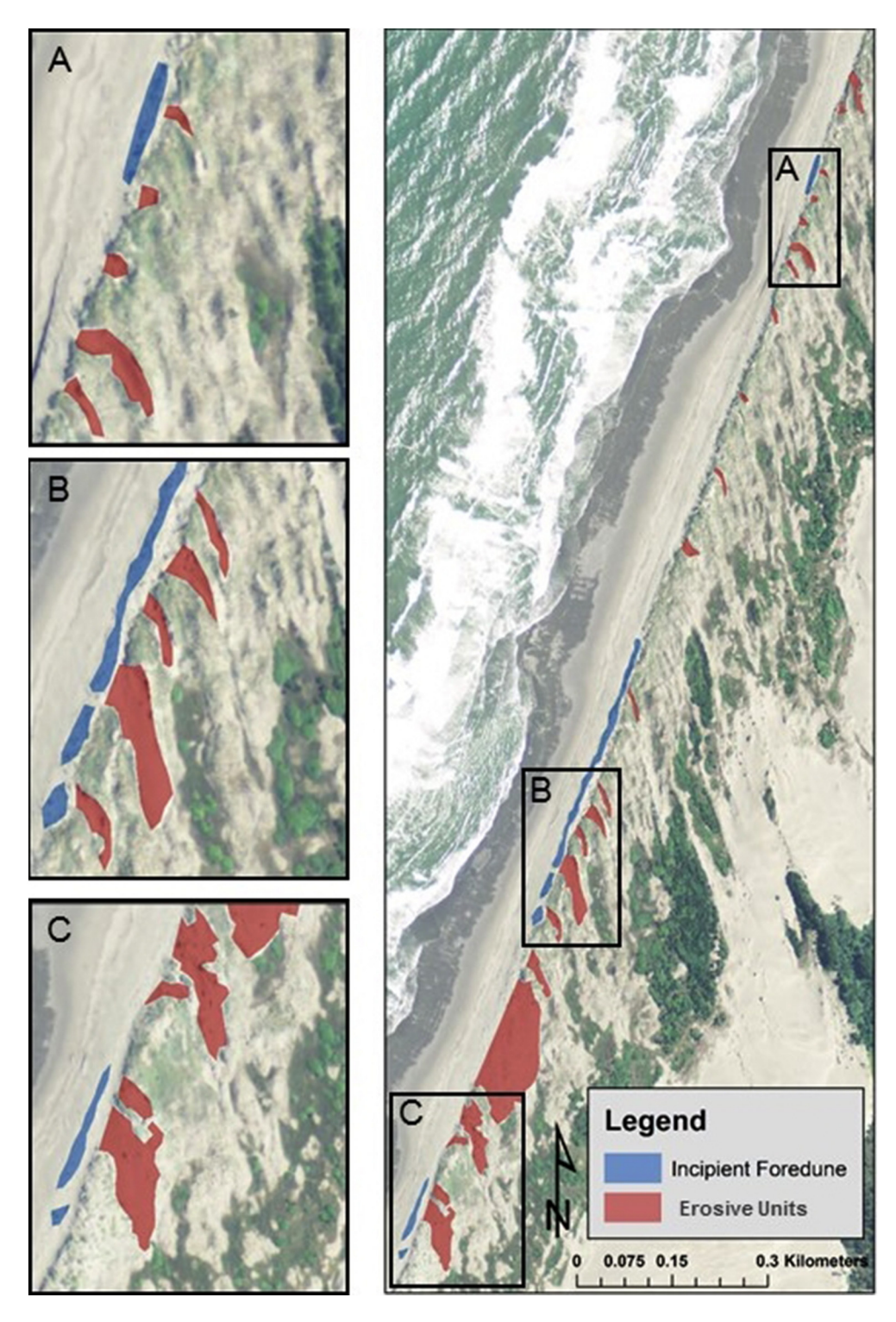


Fig. 5. Examples of mapped erosional units (principally blowouts) in the established foredune and of the incipient foredunes in front of the established foredune.

each respective zone. The differences in mean normalized area and mean normalized annual areal change between northern, central and southern geomorphic units was examined in R using one-way analysis of variance (ANOVA) (Fisher, 1935). Tukey's honest significant difference (HSD) post-hoc statistical test was performed to identify pairs of zones for which statistically significant differences in area and areal change occurred. Normalized area and annual normalized areal change of erosive units and incipient foredunes from 2004 to 2014 provide information on spatial and temporal variability in geomorphic unit evolution.

3.5. Topographic survey transects

Ten topographic transects were established in January 2012 by the US Fish and Wildlife Service (USFWS) across the study site, as outlined in Pickart (2014). Profiles vary in length from 156 to 276 m from the survey benchmarks to the water line. Surveys were conducted biannually in winter and summer seasons, with data up to July 2015 used in this study. The locations of these transects were originally chosen to represent the three foredune vegetation assemblages or 'alliances' dominant in the study area (Sawyer et al., 2009): i) *Ammophila arenaria* herbaceous alliance (transects 1, 2), ii) *Elymus* [Leymus] mollis herbaceous alliance (5, 6, 8, 9) and, iii) dune mat herbaceous alliance (3, 4, 7, 10).

Three geomorphic zones (backdune, foredune, and beach) were identified for each transect (Fig. 6). However, only the foredune and beach were used for interpreting morphological and sediment volumetric changes due to little to no volumetric change observed in the backdune during the study. The foredune zone extended cross-shore from the first point of inflection (or the basal break of slope) on the lee slope (which remained unchanged through the study period) to the seaward-most vegetation line during measurement, including the incipient foredune. The stoss toe of the foredune is typically tied to the seaward most-extent of seasonal vegetation (Hesp, 2002, 2013). As such, this line defines the boundary separating the backshore from the foredune. In contrast to the approach for foredune position change analysis, described above, the incipient foredune was included as part of the foredune zone definition as topographic profiles are able to provide more consistent and accurate delineation of foredune and beach boundary than can be obtained from the aerial photographs used here. The second zone, or unvegetated active beach, was defined by the area between the seaward vegetation line and the contour line associated with an elevation of 3.7 m above mean sea level (metres above sea level, in reference to NAVD88), a common closing point between all topographic transects at the study site to allow for sediment volumes to be compared.

Elevation data were collected from each of the 10 topographic transects bi-annually from winter 2012 to summer 2015. Topographic measurements were taken at 1-m intervals along each transect from the benchmark in the backdune to the waterline. A Trimble R10 real-time kinematic global positioning system (RTK-GPS) was used to collect elevation measurements in reference to the NAVD88. A vertical error threshold of ± 0.01 m was determined for the elevation values based on the largest reported vertical error from multiple 5-hour benchmark GPS observations.

3.5.1. Transect volume calculations

Topographic profile data were plotted (Fig. 6) and an R script was created to calculate the area underneath the entire profile, the foredune, and the beach units for each season. The volume underneath each profile surface was calculated by multiplying the vertical change in elevation measurements by $1.0~{\rm m}^2$ in area to yield a volume measurement (${\rm m}^3$). The volume calculations varied between seasons depending on the location of the seaward extent of vegetation that marked the boundary between the beach and foredune zone. As such, normalized volume measurements were calculated by dividing the seasonal volume of the foredune and beach zones by the respective transect lengths in each season, to facilitate comparison of volume changes through time.

Statistically significant differences in the total (combined beach and foredune) transect elevations, beach width, normalized volume and normalized monthly volume change between transects in the northern (1, 2, 3), central (4, 5, 6) and southern (7, 8, 9, 10) alongshore zones were analysed using ANOVA and Tukey's HSD post-hoc test. Furthermore, Welch Two Sample *t*-tests were used to test a null hypothesis that normalized monthly volume change underneath transects is independent of spatial (i.e., beach vs. foredune) and temporal (i.e., summer vs. winter) variation. The first *t*-test examined the difference between normalized monthly volume change values of all 10 transects between the beach and foredune zones. The second *t*-test examined the difference between normalized total (combined beach and foredune) monthly volume change of all 10 transects between the summer and winter monitoring periods.

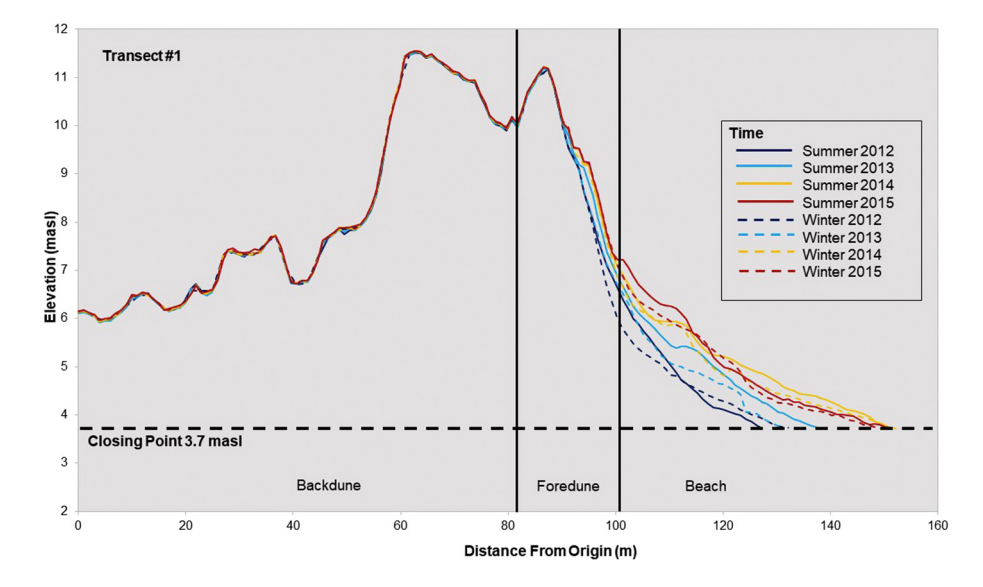


Fig. 6. An example of topographic changes at transect 1 recorded from winter 2012 to summer 2015. The extent of three geomorphic zones delineated from the winter 2012 topographic measurements indicate the backdune (which, in this case includes a stabilized older foredune ridge), foredune, and beach.

Finally, a Spearman's rank-order correlation test was performed on four variables (normalized monthly volume change in the foredune zone, normalized monthly volume change in the beach zone, alongshore zone grouping from north to south and increasing time from winter 2012 to summer 2015) in order to examine relationships between independent (time, zone) and dependent (volume change) variables that could help explain temporal and spatial variation in volume across the study site. The Spearman correlation coefficient, r, was chosen as it can evaluate monotonic relationships between continuous and ordinal data. Time and alongshore zone were ranked ordinally for simplicity and consistency to be comparable within the correlation calculation. Time was ranked from 0, representing the baseline survey in winter 2012 up to 7, the last survey interval in summer 2015, while alongshore zone was ranked from 1 in the north to 3 in the south.

4. Results

4.1. Shoreline positional change analysis

The long-term (75-year, 1939–2014) spatially averaged annual change in foredune position, or end point rate (EPR) was $-0.04~{\rm m~a^{-1}}$. Fig. 7 shows, however, that the northern portion of the foredune system prograded at rates up to $+0.51~{\rm m~a^{-1}}$, while the southern portion retreated landward at rates up to $-0.49~{\rm m~a^{-1}}$. The central zone was characterized by areas of small to negligible rates of seaward foredune migration (from +0.13 to $+0.27~{\rm m~a^{-1}}$, \pm 0.12 m ${\rm a^{-1}}$) and some areas of landward retreat (from -0.13 to $-0.35~{\rm m~a^{-1}}$, \pm 0.12 m ${\rm a^{-1}}$) (Fig. 7). The spatial clustering of change rates derived from the long-term (1939–2014) foredune position trends

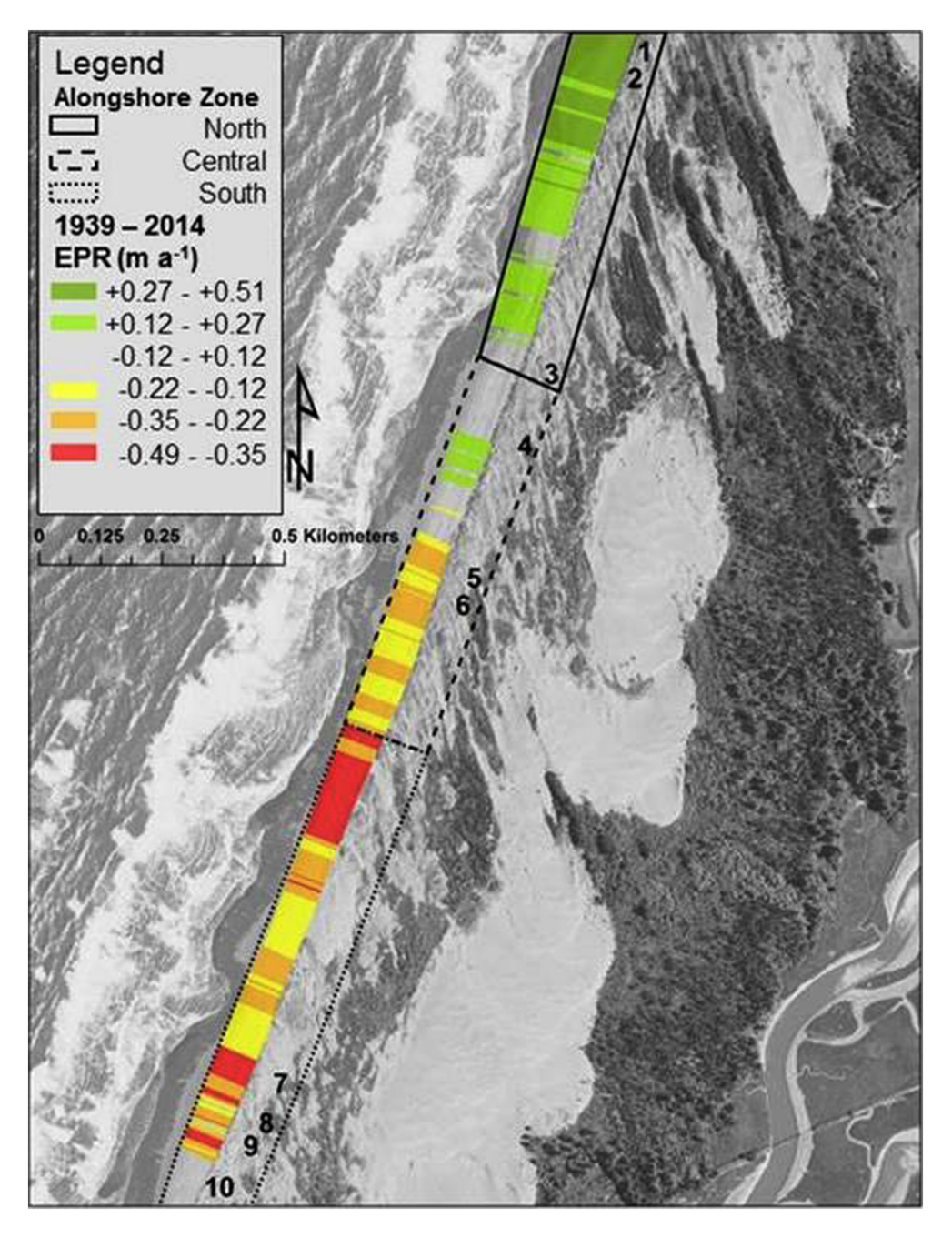


Fig. 7. Annual rates of change (end point rate, EPR in m a⁻¹) in seaward extent of the foredune across the Lanphere and Ma-le'l sand dune units from 1939 to 2014. EPR values of -0.12 to +0.12 m a⁻¹ represent insignificant change and are not represented in the figure. These data were produced using the Digital Shoreline Analysis System (DSAS) (Thieler et al., 2009). The northern, central and southern alongshore zone boundaries and transect locations 1–10 are displayed for reference.

were used to define the northern, central and southern alongshore zones used in this and other parts of the analysis (Fig. 1).

End point rate (EPR) values across the study site for 12 short-term aerial photograph intervals between 1939 and 2014 are displayed in Fig. 8. Three photo intervals (1939–1948, 2005–2009, 2012–2014) exhibit similar EPR trends as the long-term 75-year study interval, with net seaward advance of the foredune in the north to landward retreat in the south. Intervals in between 1948 and 2005 are characterized by more spatially consistent rates of foredune position change across the entire study domain, with detectable trends largely dominated by net erosion (e.g., 1948–1954, 1992–2004) or net accretion (e.g., 1965–1981, 1981–1992) with minor variation in localized spots (Fig. 8).

Fig. 9 displays the variation (distance from the median) in EPR for 8 decadal photo intervals from 1939 to 2014. The largest average EPR values are from 1954 to 1958 ($+4.19 \text{ m a}^{-1}$) and 2004–2014 (average EPR $+2.25 \,\mathrm{m\,a^{-1}}$) (Table 4, Fig. 9). Exactly half of the shorter time intervals exhibit negative average EPR values, indicative of landward retreat of the foredune (Table 4). An inset figure shows greater variation in EPR when examined at shorter, more recent intervals from 2004 to 2014 (Fig. 9). Average EPR for the northern, central and southern alongshore zones are compared in Fig. 10. In all 12 aerial photograph intervals, the largest absolute EPR values are recorded in either the north or south zones, with smaller magnitude EPR values recorded in the central zone. The southern zone experienced larger magnitude EPR values than the northern zone in 7 of 12 intervals (Fig. 10). Of these 7, the southern zone experienced negative average EPR rates, indicative of landward retreat, in 5 study intervals (Fig. 10). Additionally, 3 of the 5 interannual aerial photograph intervals from 2004 to 2014 indicate positive EPR values in the northern zone and negative EPR values in the south (Fig. 10). During three time intervals from 1965 to 2004, EPR values in all zones remained relatively similar.

4.2. Wind, wave and water level variations

Monthly average significant wave height (Hs), wave period, mean water level and maximum water levels are plotted in Fig. 11. A foredune erosional threshold value of 7.2 m was calculated for the study site from a LiDAR point cloud and displayed in Fig. 11 for reference. In general, the frequency of monthly average water level values greater than the erosional threshold increases from 1982 to 2012. Monthly average Hs and wave period values were greatest from 2001 to 2008 (Fig. 12). Fig. 12 displays monthly average Hs and MaxWL plotted against monthly average climate index values. Maximum Hs and water level values generally align with years of El Niño, as indicated by large PDO and MEI index values (Fig. 12). Additionally, large Hs values in February 1999 (4.2 m) and November 2007 (5.0 m) occur at the same time as positive NOI index values, indicative of La Niña years (Fig. 12).

4.3. Landform changes

Table 5 shows the total area and annual areal change of geomorphic units from 2004 to 2014 in the northern, central, and southern zones. Erosive units in the northern and central zones experienced alternating cycles of annual areal growth and reduction from 2004 to 2012, while southern erosive units increased steadily in area from 2004 to 2012. From 2012 to 2014, erosive units in the northern, central and southern zones experienced an annual areal decrease of -589, -776 and

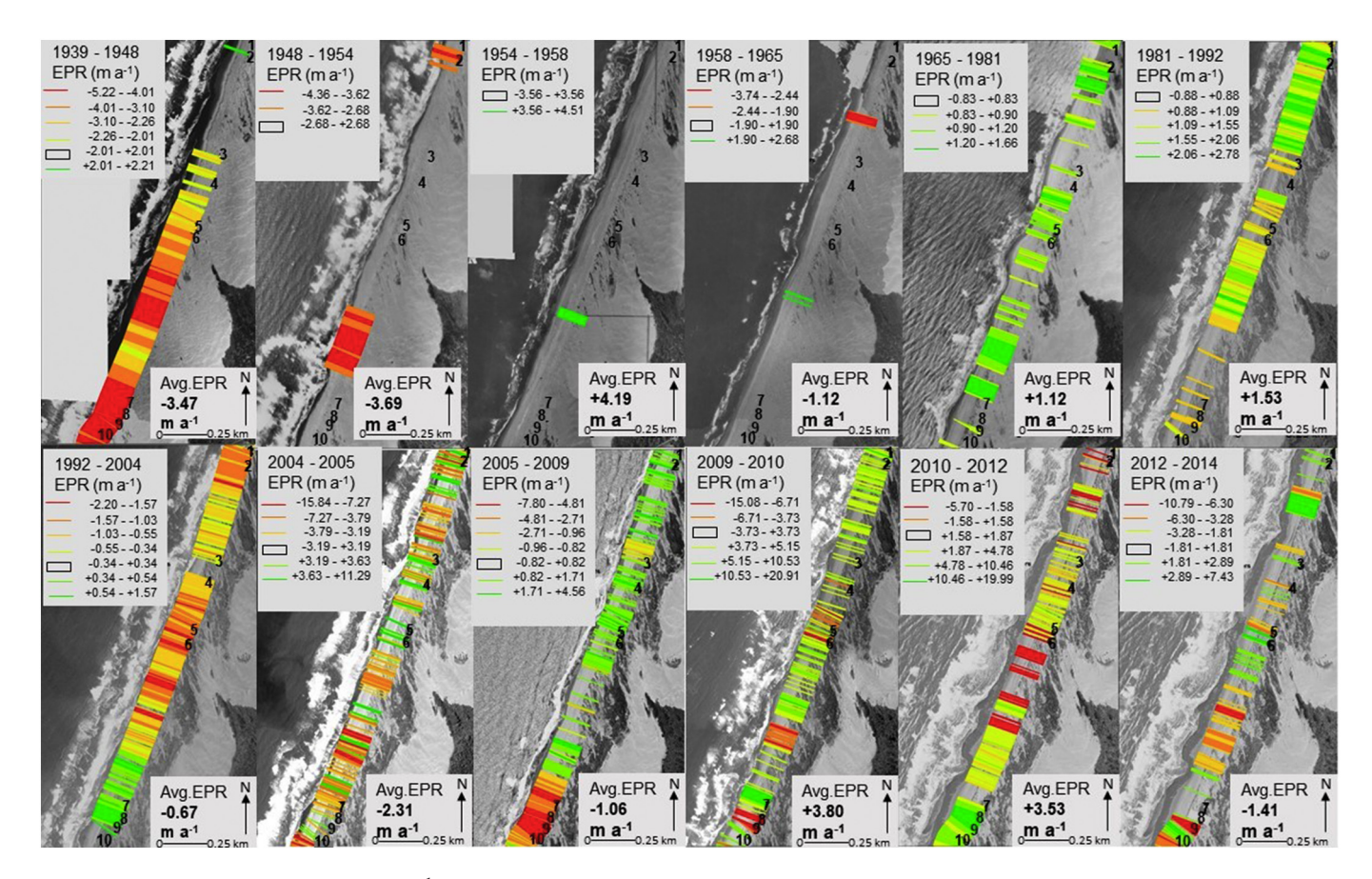


Fig. 8. Annual rate of change (end point rate, EPR m a⁻¹) in seaward extent of the foredune for 12 aerial photo intervals from 1939 to 2014. EPR values are displayed over the last aerial photograph of each study interval. Areas with no fill, as indicated by the boxed value range in the legend, represent areas of insignificant change. Transect locations are displayed for reference. Note that due to large variability in EPR values between aerial photograph intervals, EPR legends are not normalized across time intervals and similar colors do not represent similar rates of change between intervals.

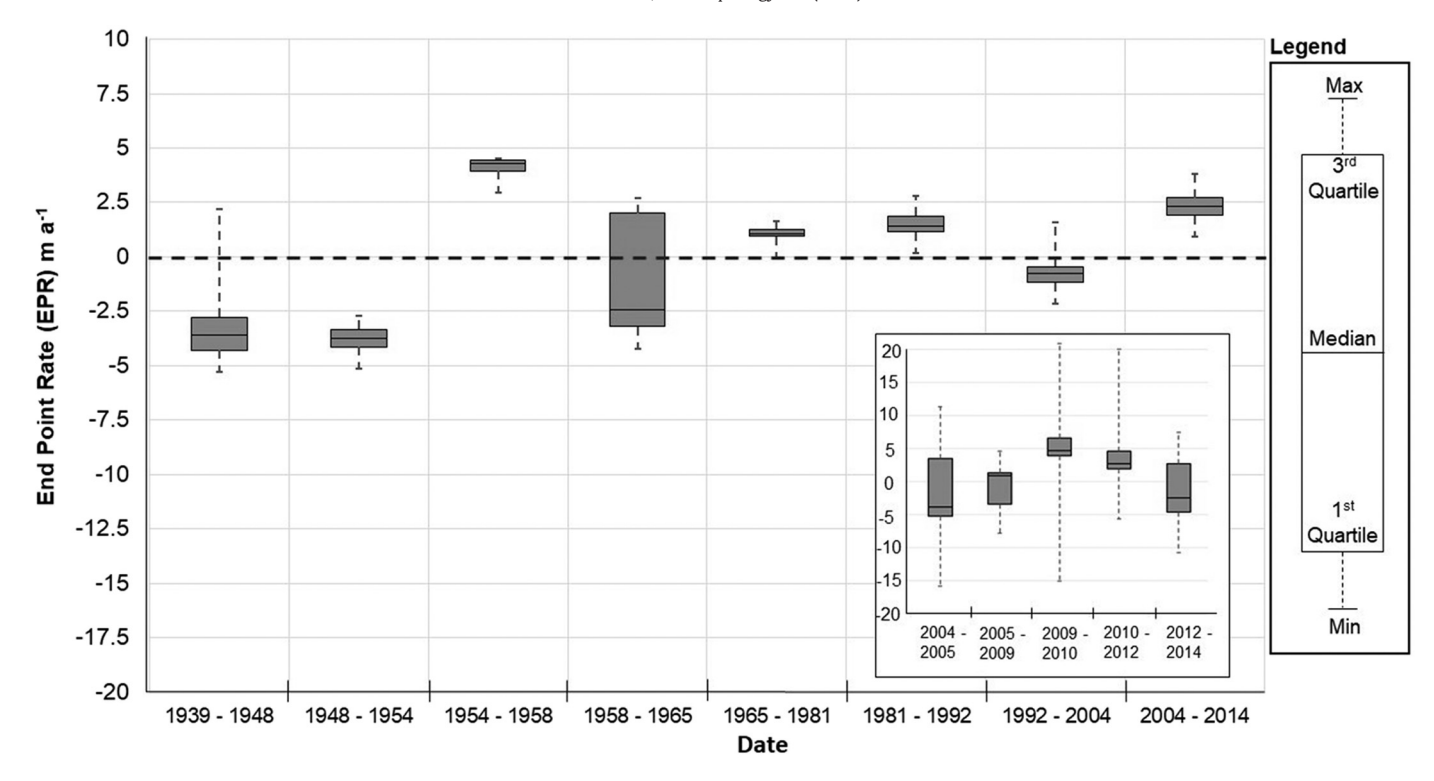


Fig. 9. Distribution of annual EPRs around median EPR values from 1939 to 2014 for 8 decadal time intervals. The lower and upper whiskers indicate the minimum and maximum EPR value for each interval, respectively. The lower box boundary and upper box boundary represents the first quartile (25th percentile) and third quartile (75th percentile), respectively. The inset plot shows the distribution of EPRs for shorter intervals from 2004 to 2014.

Table 4Minimum, median, maximum, 1st and 3rd quartile values used to create a boxplot of the distribution of annual EPR (m a⁻¹) for each photo interval from 1939 to 2014.

| - | | | | | | | | |
|-----------------------------------|-----------|-----------|-----------|-----------------|-----------|-----------|-----------|-----------|
| Date | 1939–1948 | 1948-1954 | 1954–1958 | 191,958–191,965 | 1965-1981 | 1981–1992 | 1992–2004 | 2004–2014 |
| Minimum (m a ⁻¹) | -5.2 | -4.4 | +3.6 | -3.7 | +0.8 | +0.9 | -2.2 | -0.8 |
| 1st quartile (m a ⁻¹) | -4.3 | -4.2 | +4.0 | -3.2 | +1.0 | +1.2 | -1.2 | +1.9 |
| Median ($m a^{-1}$) | -3.6 | -3.7 | +4.3 | -2.4 | +1.1 | +1.4 | -0.8 | +2.3 |
| $3rd$ quartile (m a^{-1}) | -2.8 | -3.3 | +4.5 | +2.0 | +1.3 | +1.9 | -0.5 | +2.7 |
| Maximum ($m a^{-1}$) | +2.2 | -2.7 | +4.5 | +2.7 | +1.7 | +2.8 | +1.6 | +3.8 |
| Average EPR $(m a^{-1})$ | -3.5 | -3.7 | +4.2 | -1.1 | +1.1 | +1.5 | -0.7 | +2.3 |

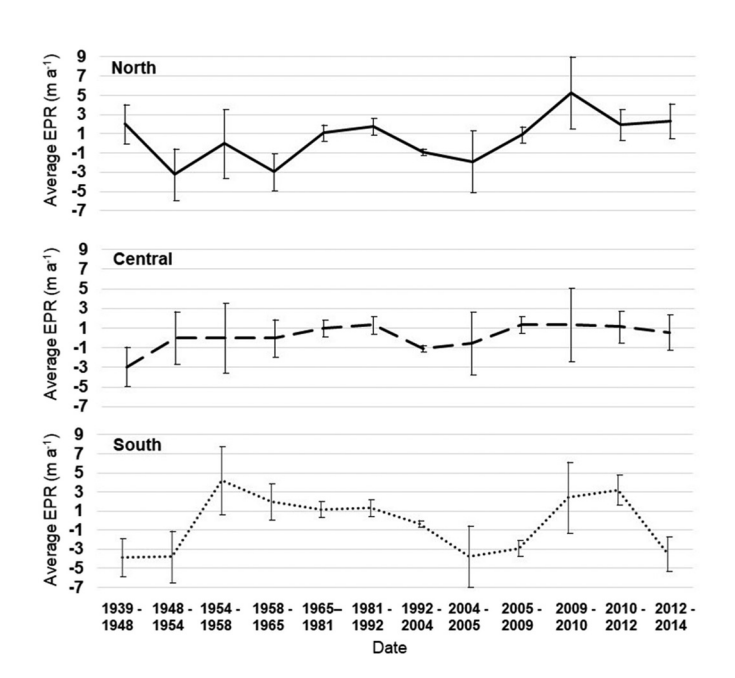


Fig. 10. Average EPR values in the northern, central and southern alongshore zones for 12 aerial photograph intervals from 1939 to 2014.

 $-2701 \text{ m}^2 \text{ a}^{-1}$, respectively. Annual areal change of incipient foredunes from 2004 to 2014 was predominantly positive across the study site.

Erosive units generally increased in area across the study site from 2004 to 2010, particularly in the central and southern zones, followed by an areal decrease from 2010 to 2014 (Fig. 13). Annual areal change of incipient foredunes across the study site appeared relatively small in magnitude ($<1000 \text{ m}^2$) from 2004 to 2012. From 2012 to 2014 the areal extent of incipient foredunes in the southern zone increased significantly ($+2404 \text{ m}^2 \text{ a}^{-1}$). The largest areal changes in both erosive units (e.g., blowouts) and incipient foredunes also occurred in the south, while the northern zone generally experienced the smallest annual areal changes in both geomorphic units (Table 5; Figs. 13 & 14).

Although the northern and central zones did not differ, ANOVA results (Table 6) show that the erosional unit area in the south was significantly larger than both the northern (p = 2.5×10^{-7}) and central zones (p = 1.4×10^{-7}). No statistically significant difference was found in mean incipient foredune area between the three zones (p = 0.12) (Fig. 14). Similarly, no difference in annual areal change of either erosive unit or incipient foredune area between zones was detected (p = 0.92 and 0.80, respectively).

4.4. Sediment volume change and statistical analysis

Minimum and maximum beach and foredune volumes for each transect are shown in Table 7. Fig. 15 shows monthly residual values from

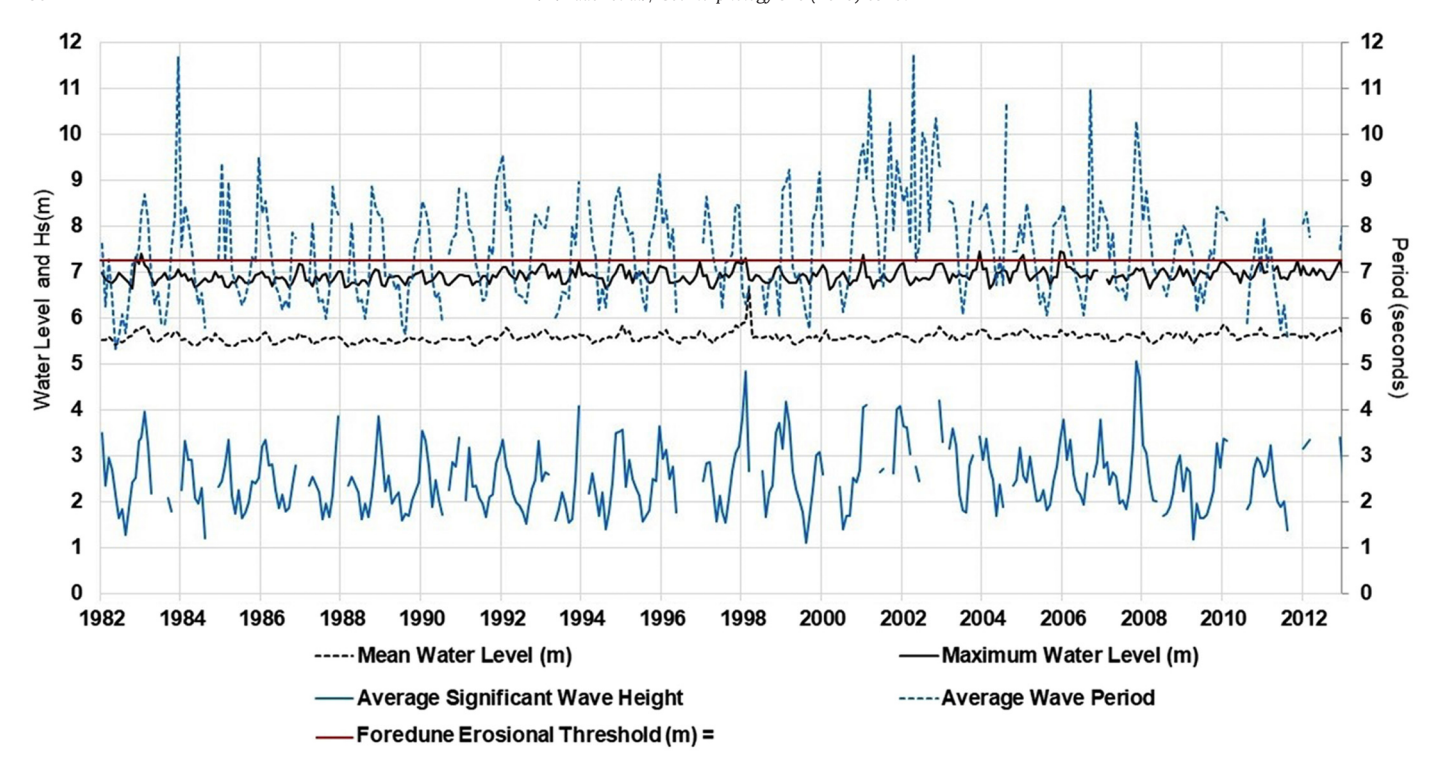


Fig. 11. Plot displaying monthly average significant wave height (m), mean and maximum water level (m) and average monthly wave period (seconds) from 1982 to 2013. The estimated foredune erosional threshold of 7.2 m, derived from LiDAR data, is displayed for reference. Wave data were recorded at NOAA buoy station 46022 at Eel River, CA (Data acquired: March 14, 2017. Data source: http://www.ndbc.noaa.gov/station_history.php?station=46022). Average monthly water level data recorded from NOAA Tidal Station 9418767 (Date acquired: March 28, 2017. Data source: https://tidesandcurrents.noaa.gov/datums.html?units=1&epoch=0&id=9418767&name=North+Spit&state=CA).

the winter 2012 to summer 2015 site-wide average rate of foredune and beach volume change. Residual values of the average monthly rate of volume change that deviate the most from the site-wide average in

the foredune (1.8 m³ mo⁻¹) and the beach (2.2 m³ mo⁻¹) are found in transect 9, while transects 2 and 10 display the smallest deviations in foredune and beach volume change, respectively. Fairly consistent

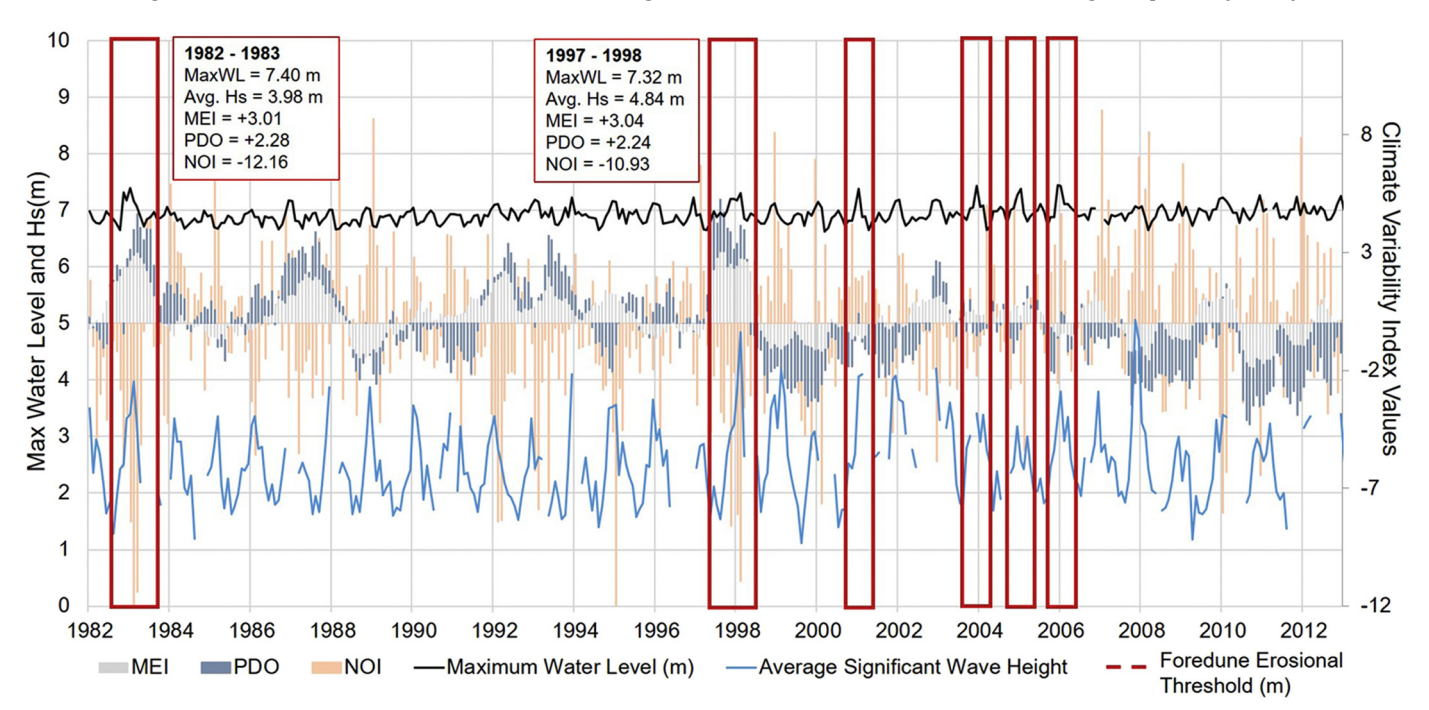


Fig. 12. Time series displaying average monthly significant wave height (m) and maximum water level (m) plotted against a stacked bar graph of three climate variability (CV) index values MEI, PDO, NOI. Boxes are drawn around time periods that exhibit MaxWL over the estimated erosional threshold elevation for foredunes at the study site. Maximum wave, water level, and CV index values for two periods regularly referenced for particularly extreme El Niño events (1982–83, 1997–98) are indicated. Wave data were recorded at NOAA buoy station 46022 at Eel River, CA (Data acquired: March 14, 2017. Data source: http://www.ndbc.noaa.gov/station_history.php?station=46022). Average monthly water level data recorded from NOAA Tidal Station 9418767 (Date acquired: March 28, 2017. Data source: https://tidesandcurrents.noaa.gov/datums.html?units=1&epoch=0&id=9418767&name=North+Spit&state=CA). Climate Index data acquired from NOAA Earth System Research Laboratory (Data acquired: March 28, 2017. Data source: https://www.esrl.noaa.gov/psd/data/climateindices/list/).

Table 5 Total area (m^2) and annual areal change $(m^2 a^{-1})$ of geomorphic units (erosive units and incipient foredunes) in the northern, central and southern zones.

| Date | Total area (m²) | Change in area (m² a ⁻¹) | Total area (m²) | Change in area (m² a ⁻¹) | Total area (m²) | Change in area (m² a ⁻¹) |
|--------|-----------------------|--|-----------------------|--|-----------------------|--|
| Northe | rn erosiv | e units | Central e | osive units | Southern | erosive units |
| 2004 | 1592 | _ | 1513 | _ | 9546 | _ |
| 2005 | 2449 | +857 | 3241 | +1728 | 11,340 | +1794 |
| 2009 | 1417 | -258 | 1885 | -339 | 18,403 | +1766 |
| 2010 | 2607 | +1190 | 3407 | +1522 | 22,262 | +3859 |
| 2012 | 1983 | -312 | +1903 | -752 | 23,112 | +425 |
| 2014 | 805 | -589 | 352 | -776 | 17,710 | -2701 |
| Northe | rn incipie | ent | Central in | cipient | Southern | incipient |
| foredu | ne | | foredunes | 3 | foredunes | |
| 2004 | 0 | _ | 296 | _ | 529 | - |
| 2005 | 0 | 0 | 1218 | +922 | 402 | -118 |
| 2009 | 303 | +76 | 3541 | +581 | 970 | +142 |
| 2010 | 675 | +372 | 3325 | -216 | 313 | -657 |
| 2012 | 477 | -99 | 3061 | -132 | 1496 | +592 |
| 2014 | 2124 | +824 | 3858 | +399 | 6304 | +2404 |

rates of residual volume change in both the foredune and beach are seen in transects 2–4. Transects 5 and 6 are characterized by small scale monthly decreases in residual foredune and beach volume change (Fig. 15). In the southern zone, transects 7–10 demonstrate variable rates of residual volume change (Fig. 15).

ANOVA and Tukey HSD tests were performed to identify statistically significant differences in mean total (combined beach and foredune) transect elevation, mean beach width, mean normalized foredune and beach volumes and mean normalized foredune and beach monthly volume changes between northern, central and southern transects (Table 8). The mean total transect elevation and mean foredune volume are greater in the northern and central zones than in the south (p values 2.0×10^{-16} and 6.0×10^{-9} , respectively). However, there is no significant difference in beach width, total volume, beach volume or normalized monthly volume changes in either beach or foredunes between alongshore zones.

A Welch Two Sample *t*-test demonstrated no statistically significant difference in average normalized monthly volume change between the beach and foredunes zones of all 10 transects. A second *t*-test demonstrated a statistically significant (p-value <0.05) difference between monthly normalized volume change in the

summer (mean of $-0.04 \, \mathrm{m^3 \, mo^{-1}}$) and winter seasons (mean of $+0.05 \, \mathrm{m^3 \, mo^{-1}}$). Site-wide volume changes in both the beach and foredune zones are positively but weakly correlated with time, producing r values of 0.2 and 0.1, respectively (Fig. 15). An r value of 0.4 indicates that the monthly site-wide foredune volume change is weakly positively correlated with monthly site-wide beach volume change (Fig. 15).

5. Discussion

5.1. Long-term changes in established foredune position

The rate of foredune position change, as defined by the average position of the visible foredune vegetation line over the 75-year study period, is characterized by an alongshore gradient (Fig. 7) with maximum foredune progradation of $+0.51~{\rm m~a^{-1}}$ in the north and foredune retreat ($-0.49~{\rm m~a^{-1}}$) in the south. Insignificant foredune position change in the northern half of the central zone transitions to small-scale landward retreat in the central-south zone boundary (Fig. 7). Thus, the central zone represents a transitional regime in regard to the varying effects that aeolian transport, longshore littoral drift, and morphological sediment budget processes have on foredune position.

A regional scale study (Hapke et al., 2006) of short-term shoreline change for the Eureka region (extending from 6 km south of Trinidad Head to Cape Mendocino; Fig. 1) reported a similar north to south gradient in regional shoreline position, although there was a large data gap near the North and South spits of Humboldt Bay. This was attributed to long-term shoreline change patterns in the larger Eureka Littoral Cell to directional variations in waves and currents (Hapke et al., 2006, 2009). At the study site, seasonal wave regimes are dominated by northwesterly wind waves $(280^{\circ}-330^{\circ}, 1-4 \text{ m}, 3-10 \text{ s})$ during the summer and North Pacific swell (210°-350°, 2-10 m, 10-25 s) in the winter (Table 1, Fig. 3) (Storlazzi and Wingfield, 2005). Along most of the California coastline, seasonal summer northwest wind waves and winter Pacific swell waves combine with the California Current to drive net sediment transport to the south in most littoral cells (Storlazzi and Wingfield, 2005; Hapke et al., 2006, 2009). The Eureka Littoral Cell deviates from this trend with alongshore sediment transport to the north in association with the southward migration of the Hawaiian High Pressure system during the winter (Hapke et al., 2006. 2009). Rivers act as a primary source of coastal sediment with an average of 70-95% of beach sand in California being delivered from coastal

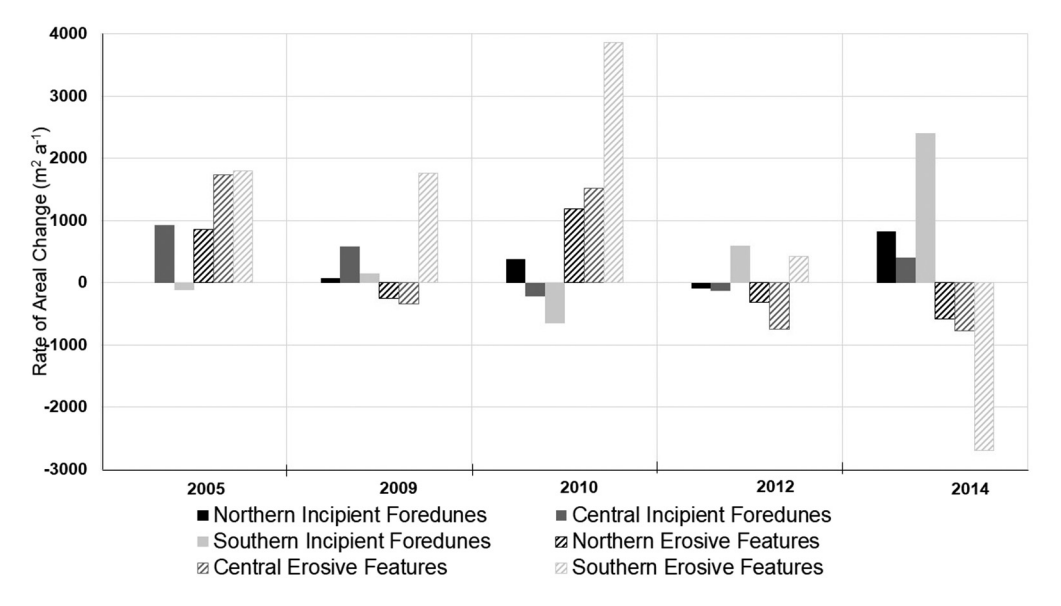


Fig. 13. Changes in average annual areal coverage of geomorphic units across the entire study area as calculated from geomorphic mapping based on aerial photograph analysis.

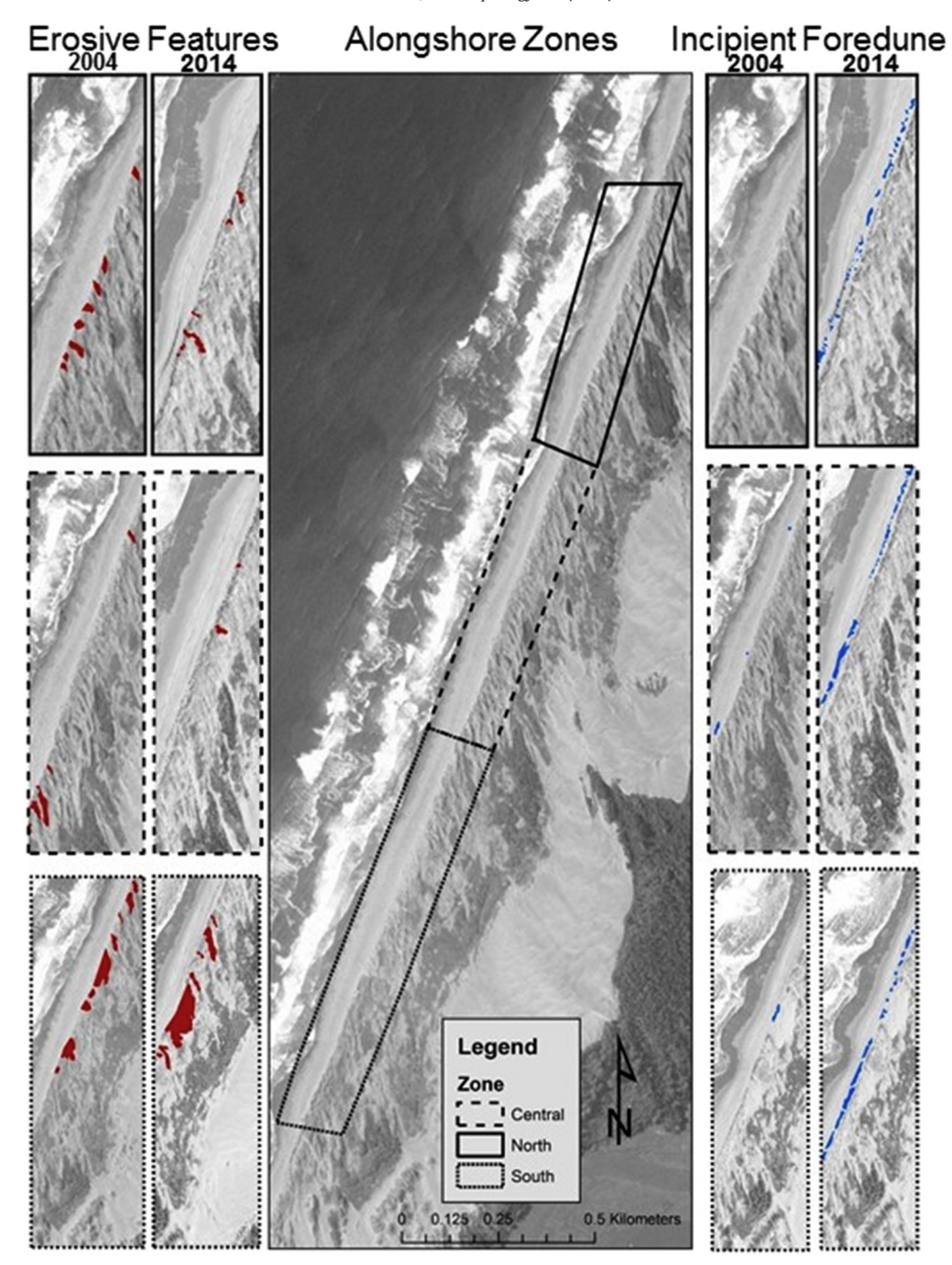


Fig. 14. Change in erosive units (principally blowouts; left columns) and incipient foredunes (right columns). Smaller outer panels display example segments of geomorphic units from the northern, central and southern zones in 2004 and 2014.

streams (Runyan and Griggs, 2003; Hapke et al., 2006). Although the exact contribution of sediment to the littoral system remains unknown at this site, Wheatcroft and Sommerfield (2005) suggest that large suspended sediment fluxes from the Eel River, to the south of the study site, and the Mad River, to the north of the study site, are significant sources of sediment to the littoral system, and thus, to the beaches and coastal dunes.

The presence of an extensive transgressive dune system on the North Spit of Humboldt Bay is consistent with significant sediment supply over the Holocene from the Mad River, which also offers possible explanation for the north to south gradient in beach-dune response captured in the photo analysis and for the statistical difference in foredune morphology identified in the seasonal topographic profiles. The

combined effects of sediment retention on the coastal shelf just north of the study site at the mouth of the Mad River (Fig. 1) and dominant north to south littoral drift during the summer might result in a sediment supply gradient, decreasing toward the south. Consequently, less sediment is available to be cycled on - and - offshore in the south, effecting foredune size, position, and morphology (de Vries et al., 2012). Although beyond the *meso* spatial scales (100s of metres to kilometres) and temporal scales (annual to decadal) of this study, there are other plausible and linked contributions to this observed gradient in geomorphic and sediment budget response, including: i) an observed increase in monthly mean relative sea level (+4.7 mm a⁻¹, station 9418767 at North Spit, CA), ii) a regional N to S gradient in interseismic land level change associated with the Cascadia subduction

Table 6Summary of ANOVA and Tukey HSD test results for significant differences in area (m²) and annual areal change (m² a⁻¹) between geomorphic units in the northern, central and southern alongshore zones.

| Location | North | Central | South | North | Central | South |
|-------------------------|---|----------------------|----------------------|--|-----------------------|---------------|
| | Normalized erosive | unit area (m²) | | Normalized incipien | t foredunes area (m²) | |
| Mean | 0.09 | 0.15 | 1.3 | 0.03 | 0.18 | 0.13 |
| ANOVA p value | 4.9×10^{-7} | | | 0.12 | | |
| Statistically different | ✓ | | | X | | |
| Tukey HSD comparison | North-Central | North-South | Central-South | North-Central | North-South | Central-South |
| p value | 0.93 | 2.5×10^{-7} | 1.4×10^{-7} | - | - | - |
| Statistically different | X | ✓ | ✓ | - | - | - |
| | Annual change in normalized area of erosive unit $(m^2 a^{-1})$ | | | Annual change in normalized area of incipient foredune (m ² a | | |
| Mean | +0.01 | +0.02 | +0.02 | +0.01 | +0.02 | +0.04 |
| ANOVA p value | 0.92 | | | 0.80 | | |
| Statistically different | X | | | X | | |

Table 7Minimum, maximum and average volume (m^3) in the foredune and beach zones of transects 1–10 across all monitoring periods (winter 2012–summer 2015). The rate of volume change statistics $(\pm 0.01 \text{ m}^3 \text{ mo}^{-1})$ in the foredune and beach are listed in brackets for all transects.

| Foredune transect | Min. volume | Max. volume | Mean SE \pm 202.71 (m ³) | Beach transect | Min. volume | Max. volume | Mean SE ± 47.56 (m ³) |
|-----------------------|---------------|---------------|--|----------------|---------------|----------------|-----------------------------------|
| Northern transect vol | umes (m³) | | | | | | |
| 1 | 150.3 (-15.7) | 355.6 (+16.5) | 241.4 (+2.7) | 1 | 100.1 (-10.7) | 167.8 (+10.3) | 149.1 (+0.3) |
| 2 | 209.3(+0.3) | 275.8 (+7.2) | 257.8 (+1.6) | 2 | 53.1 (-8.2) | 293.5 (+21.6) | 144.3 (+4.6) |
| 3 | 756.0 (-9.5) | 813.0 (+2.2) | 781.6 (-0.3) | 3 | 0.0 (-21.3) | 326.3 (+20.6) | 186.9 (+4.7) |
| Central transect volu | nes (m³) | | | | | | |
| 4 | 591.6 (-8.9) | 652.3 (+6.0) | 615.0 (-0.1) | 4 | 45.6(-5.6) | 253.8 (+22.4) | 159.8 (+4.3) |
| 5 | 847.3 (-11.8) | 953.3 (+14.4) | 912.4 (+0.6) | 5 | 44.0 (-10.3) | 182.8 (+21.1) | 114.9 (+1.7) |
| 6 | 533.0 (-4.2) | 617.4 (+11.2) | 571.3 (+1.5) | 6 | 35.4 (-19.3) | 198.5 (+16.9) | 126.9 (+0.5) |
| Southern transect vol | umes (m³) | | | | | | |
| 7 | 426.5(-6.8) | 607.0 (+20.9) | 553.9 (+3.5) | 7 | 46.7 (-114.3) | 209.6 (+131.8) | 128.3 (+5.8) |
| 8 | 564.8 (-9.6) | 632.9 (+9.8) | 594.0 (+1.5) | 8 | 65.9 (-11.8) | 200.0 (+21.1) | 133.5 (+0.5) |
| 9 | 252.8 (-0.7) | 502.7 (+36.4) | 461.2 (+6.0) | 9 | 79.5 (-33.4) | 279.9 (+12.3) | 156.9 (-2.2) |
| 10 | 686.9 (-8.7) | 800.5 (+8.9) | 746.3 (+1.5) | 10 | 88.9 (-8.5) | 200.9 (+13.9) | 145.4 (+2.1) |

zone (Williams et al., 2013), iii) evidence of relative sea- level changes in the late Holocene (Engelhart et al., 2015), and iv) unknown variations in nearshore bathymetry (Houser et al., 2008; Houser, 2012). These factors provide an opportunity for future research regarding thresholds of coastal change related to larger scale processes in the Eureka Littoral Cell. In turn, findings from such work could help coastal managers prioritize risks to, and drivers of, regional foredune change.

5.2. Recent interannual changes in foredune position and morphodynamics

A distinct climatic shift in CV index values, such as PDO, is thought to have occurred in the late 1970s, resulting in more frequent and stronger storms linked to widespread erosion of sandy shorelines (Storlazzi et al., 2000; Allan and Komar, 2002; Storlazzi and Wingfield, 2005; Hapke et al., 2006, 2009). Following a shift to positive PDO values in 1977,

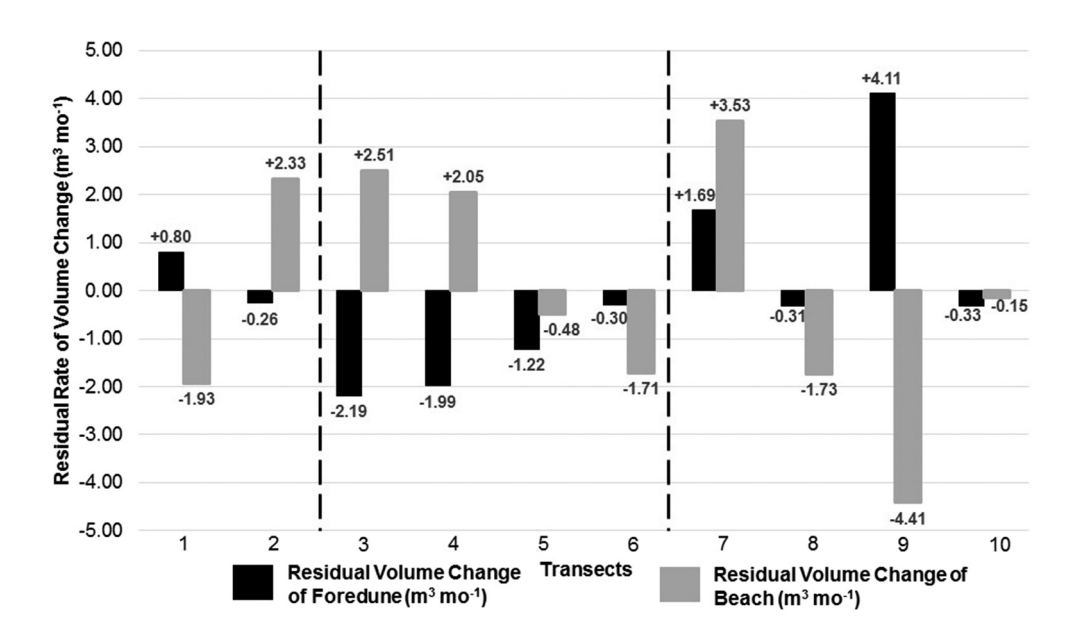


Fig. 15. Residuals of monthly volume change (m³ mo⁻¹) for each transect from the long term (winter 2012–summer 2015) average rate of monthly volume change across all transects. Dotted lines indicate the boundary lines for the northern, central and southern zones.

Table 8Summary of ANOVA and Tukey HSD results testing for significant differences in total (beach and foredune) transect volume (m³) and monthly total volume change (m³ mo⁻¹), normalized foredune volume (m³) and volume change (m³ mo⁻¹) and normalized beach volume (m³) and volume change (m³ mo⁻¹) between northern, central and southern alongshore zones.

| Location | North | Central | South | North | Central | South | |
|-------------------------|----------------------|-----------------------------------|----------------------|---|---------------------------------|---------------|--|
| | Total transect volu | me (m³) | | Total transect volum | e change (m³ mo ⁻¹) | | |
| Mean | 587.0 | 833.4 | 674.6 | 4.5 | 2.8 | 3.7 | |
| ANOVA p value | 0.4 | | | 0.9 | | | |
| Statistically different | X | | | X | | | |
| | Normalized foredu | ne transect volume (m | ³) | Normalized foredune transect volume change (m ³ mo ⁻¹) | | | |
| Mean | 9.2 | 9.0 | 8.0 | -0.0 | 0.0 | -0.1 | |
| ANOVA p value | 6.0×10^{-9} | | | 1.0 | | | |
| Statistically different | ✓ | | | X | | | |
| Tukey HSD comparison | North-Central | North-South | Central-South | North-Central | North-South | Central-South | |
| p value | 0.5 | 0.0 | 4.1×10^{-6} | _ | _ | _ | |
| Statistically different | X | ✓ | ✓ | - | - | - | |
| | Normalized beach | transect volume (m ³) | | Normalized beach transect volume change (m ³ mo ⁻¹) | | | |
| Mean | 4.3 | 4.3 | 4.4 | +0.6 | +0.8 | +0.0 | |
| ANOVA p value | 0.8 | | | 1.0 | | | |
| Statistically different | X | | | X | | | |

subsequent El Niño and La Niña events have been relatively more extreme, with a general increase in maximum water level values and particularly high intensity wave events, for example, during the winter months of 1982/83 and 1997/98 (Fig. 12) (Storlazzi et al., 2000; Sallenger et al., 2002; Allan and Komar, 2002). Often, El Niño is followed

by a strong La Niña phase (positive NOI and negative MEI values), such as that in 1998/99 (Fig. 12) (Allan and Komar, 2002). Typically, during El Niño and positive PDO events, sea surface temperatures increase in the coastal northeastern Pacific Ocean and atmospheric circulation patterns weaken, yielding higher water levels along the coast of California that

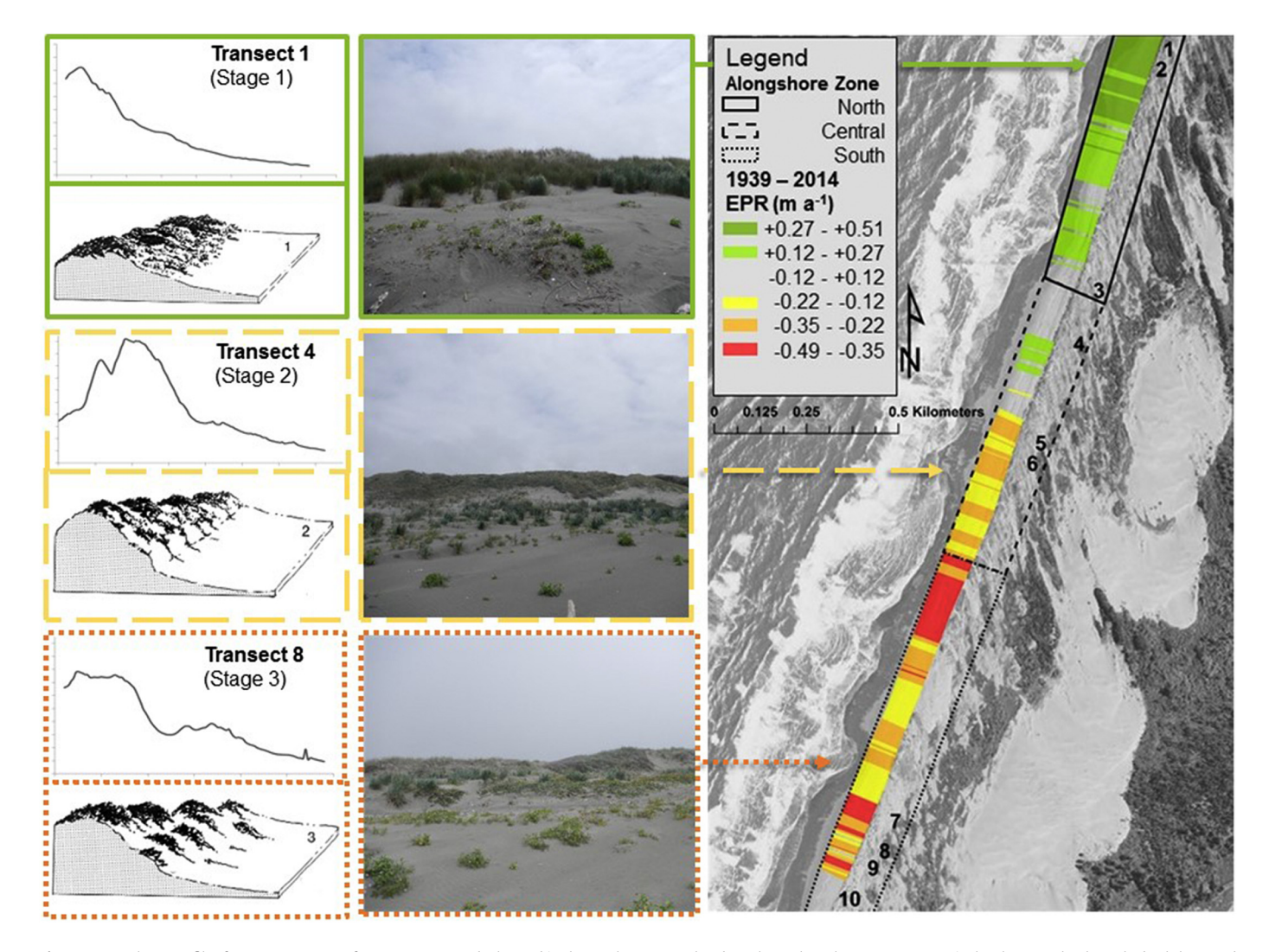


Fig. 16. Cross-shore profiles from summer 2015 for transect 1, 4 and 8 located in the northern, central and southern alongshore zones respectively. Photographs show the backshore and foredune morphologies of corresponding transects. Cross-shore profiles and photographs are set next to diagrams of foredune development stages 1–3, produced in Hesp (1988a, b).

can contribute to beach erosion. For example, studies from the central and southern California coast indicate significant flooding and erosion during El Niño periods from 1982/83 and 1997/98 (Storlazzi and Griggs, 2000; Barnard et al., 2017). However, coastal response to these events appears to have varied from the recorded trends along the south and central coasts, with storm energies during the 1998/99 La Niña resulting in higher rates of shoreline erosion at the study site than its preceding El Niño periods, as seen in the 1992–2004 shoreline change interval (Fig. 8). During this interval, site-wide foredune retreat was observed, with an average EPR of $-0.67~\mathrm{m~a}^{-1}$.

Previous studies indicate that blowout contraction may occur through re-vegetation as incipient foredune growth and/or pioneer plant communities interrupt wind flow patterns within blowouts (Gares and Nordstrom, 1995; Hesp, 2002; Abhar et al., 2015). At this site, an increase in incipient foredune area occurred alongside the stabilization and general healing of erosive units between 2012 and 2014 in all three zones (Figs. 13, 14). However, the extent of erosive unit response to incipient foredune areal increase and vegetation stabilization varies between the northern and southern zones. For example, although there was a decrease in erosive unit area, the largest erosive units, clustered in the southern zone, joined together and extended landward (Fig. 14). Stabilization of certain parts of blowouts may result in the extension and enlargement of blowouts in another direction or portion of the blowout, depending on local scale factors such as vegetation growth patterns, sediment availability and wind flow (Hesp, 2002; Abhar et al., 2015). A north to south gradient in sediment availability and localized flow patterns in the larger transgressive dune system could explain some of the morphodynamic responses at the southern end of the study site. Here, the largest erosive units continue to extend landward into the transgressive dune field, and more sediment is stored in the incipient and established foredunes (Fig. 14). Additionally, this might reflect spatial variation in foredune stabilization and developmental stages (cf. Hesp, 1988a, b), with erosive unit expansion in the south and healing in the north.

5.3. Spatial variability in established foredune development

Hesp (1988a, b, 2002) proposed five stages of foredune development that progress from stage 1 foredunes, characterized by simple topography (topographically continuous, gently undulating) and dense vegetation, to stage 5 foredunes, characterized by the presence of remnant knolls, blowouts, small sand sheets, and sparse vegetation cover. The stages of foredune development represent a measure of stability of the foredune, as determined by sediment supply, long-term sedimentation patterns and morphological characteristics (beach width, height, volume) (Hesp, 2002). At the study site, foredunes in the north exhibit statistically larger seasonal foredune elevations and volumes then those in the southern zone (Table 8). Additionally, residual volume change values in the beach are predominantly positive in the north (i.e., transects 2 and 3) and highly variable with both maximum and minimum residual volume change values in the south (Fig. 15).

In the context of this model, the northernmost foredunes are similar to stage 1 foredunes, with a dense vegetation cover (90–100% of both invasive A. arenaria and native dune grass species), and the observed pattern of sediment accumulation likely due to a net positive sediment input into the beach, resulting in long-term foredune progradation (up to $+0.51 \text{ m a}^{-1}$) (Figs. 7, 16). Farther south, foredunes transition into more dynamic, lower and hummocky morphologies, or Hesp's stage 3, where maximum landward retreat of the foredune (up to -0.49 m a^{-1}), a statistically significant larger erosive unit area and visible erosive unit areal expansion is observed (Table 5, Fig. 15). Additionally, vegetation coverage on the southern dunes is less dense than those in the north, partially due to more recent invasive vegetation management projects and dune ecosystem restoration activities (Pickart and Barbour, 2007; Pickart, 2013, 2014). The central zone may be considered a transition zone between northern stage 1 foredunes and stage

3 foredunes in the south, exhibiting statistically similar height, volume and geomorphic unit evolution values as northern stage 1 foredunes (Tables 5, 8), and foredune position change values ranging from insignificant to small scale landward retreat (Fig. 7). Hesp (1988a, b, 2002) suggest that foredunes may evolve to different stages of development following erosive events (e.g., major wave scarping, blowout formation, and/or vegetation dieback), or accretional events (rebuilding through revegetation and sediment infill). With measures of elevation and volume characteristics being relatively equal between the northern and central foredunes, central foredunes may be continually transitioning between stage 1 and stage 2 foredunes based on alongshore variation in littoral drift and sediment supply patterns following seasonal storm events (Hesp, 2002) (Fig. 7).

The observed gradient of generally stable foredunes in the north to more dynamic foredunes in the south and related foredune developmental stages might be dominantly related to interactions between sediment supply, surf zone type, and beach-dune dynamics (Short and Hesp, 1982; Hesp, 1988a, b, 2002; Arens, 1996). Previous studies (Cooper, 1967; Psuty, 1988) suggest that foredune development may be a product of proximity to sediment source (e.g. river discharged sediment) and temporal variations in climate patterns that can alter sediment transport patterns. As such, the north to south gradient in foredune development (Fig. 16) may result from alongshore variation in offshore sediment supply and transport following seasonal shifts in wave and aeolian transport energies. Across all transects examined in this study, seasonal volume changes were significantly greater in the beach zone than seasonal volume change in the established foredune, and greater in the winter season than in the summer season. Many studies show that the sediment volumes of beaches fluctuate greatly on a seasonal basis (Sherman and Bauer, 1993; Anthony et al., 2006; Ruggiero et al., 2010).

Summer northwest wind waves coupled with dominant littoral circulation to the south results in sediment being transported largely into the northern beach zone (Fig. 2) (Harris et al., 2005; Storlazzi and Wingfield, 2005; Warrick, 2014). Higher sediment transport potential from the beach to the foredune, and through aeolian transport out of the NNW, supports the increase in dune ridge elevation and development of stage 1 foredunes in the north (Fig. 7) (cf. Psuty, 1988). Alternatively, lower sediment availability in the southern zone could result in smaller sediment inputs to the beach during the summer months, in turn resulting in topographic dune units with lower average elevations, such as the stage 3 foredunes (cf. Psuty, 1988). As such, erosive events fuelled by North Pacific swell coming out of the west and high-water levels may result in seasonal destabilisation of the foredune at the study site, particularly in the south, where foredunes are characterized by lower volumes and lower elevations (Fig. 3, Table 8) (Storlazzi and Wingfield, 2005). With the return of summer littoral dynamics, foredunes in the north are replenished with higher offshore sediment supplies and transport potential into the beach, while limited sediment availability in the south lowers the opportunity for full foredune recovery, perpetuating the north to south trend in foredune development.

6. Conclusions

Historic patterns in foredune position and evolution of morphodynamic units, along with interannual sediment budget (volumetric) responses were analysed at the Lanphere and Ma-le'l Dune units in HBNWR. These data allow an assessment of the various stages of morphological development of foredunes and associated landform units across the study site. Identifying trends between datasets of multiple temporal and spatial resolutions points to general morphodynamic processes effecting foredune development and local morphological variability. Key findings of this study include:

 Rates of annual foredune position change vary across the study site, exhibiting a north to south erosional gradient with the highest rate of foredune advance (+0.51 m yr⁻¹) occurring in the north and the highest rate of foredune retreat of $-0.49~{\rm m~yr^{-1}}$ in the south. The central zone was characterized by areas of negligible foredune position change and slow rates of seaward foredune migration (from $+0.13~{\rm to}~+0.27~{\rm m~a^{-1}}, \pm 0.12~{\rm m~a^{-1}})$ or landward retreat (from $-0.13~{\rm to}~-0.35~{\rm m~a^{-1}}, \pm 0.12~{\rm m~a^{-1}})$. Variability in long-term (75 year) trends of foredune position from the site-wide average speaks to the role of scale and data aggregation in generalizing the spatiality of morphodynamic processes. For example, a north to south trend in foredune position is partially fuelled by seasonal variations in littoral drift processes characteristic of the Eureka Littoral Cell, with dominant wind, wave and current dynamics driving littoral sediment transport from the north to the south in the summer and vice versa during winter storms and El Niño years. Future studies would benefit from multi-scalar examination, as common trends may help identify local drivers of morphodynamic change.

- 2. Examination of foredune position at 12 shorter-term aerial photograph intervals between 1939 and 2014 revealed that 3 intervals (1939–1948, 2005–2009, 2012–2014) exhibited similar EPR trends to the long-term 75-year study interval. An examination at smaller time intervals exhibits high variability in foredune position change in more recent intervals (from 2004 to 2014). Higher variability in foredune position may be a geomorphic response to more recent extreme climate variability events. Storm conditions during these seasons have been shown to alter dominant wind and wave directions and, in turn, might interrupt broader scale littoral drift and aeolian activity regimes that control foredune position and morphodynamics.
- 3. Recent interannual results from 2004 to 2014 suggest that the development of erosional units may be a morphodynamic response to both sediment availability and areal increase of incipient foredunes. Hypothetically sediment supply to the beach allows for the seaward spread of pioneer vegetation and the greater development of incipient foredunes. Appreciable sediment delivered to the northern beaches facilitates closing of the mouths of blowouts in the north through vegetation establishment and sediment deposition. However, partially driven by a sediment supply gradient, lower sediment inputs in the south results in less material to facilitate erosive unit healing, and greater potential for seasonal destabilisation despite the presence of an incipient foredune. Thus, aeolian processes continue to operate within the established foredune complex in the south, causing landward extension of blowouts between stabilizing vegetation.
- 4. Foredune position change trends and geomorphic responses indicate a north to south gradient in foredune evolution, with stage 1 foredunes in the north transitioning to stage 3 foredunes in the south. Developmental stages are likely fuelled by variations in seasonal sediment inputs into the beach zone and resulting volumetric increases of beach and foredune units by aeolian transport. Foredune volumes in the south are disproportionately affected by winter storm energies and experience longer recovery intervals, most likely due to lower availability of sediment. As such, foredunes in the south might be unable to recover fully in summer months, limiting the opportunity for re-vegetation and development back toward a stage 2 morphology.

Acknowledgements

Alana Rader would like to thank the University of Victoria and the U.S. Fish and Wildlife Service (USFWS), Humboldt Bay National Wildlife Refuge for financial and logistical support for this project. Thanks are also extended to the Rutgers Coastal Climate Risk and Resiliency (C2R2) traineeship program for support during revision stages. Further acknowledgements to Michael Grilliot and Derek Heathfield for support in field data collection and processing. Ian Walker acknowledges research support funding from the Natural Sciences and Engineering Research Council (NSERC) of Canada's Discovery Grant program (award

no. 239751-2011), the Canada Foundation for Innovation (CFI) Leader's Opportunity Fund (projects #4632 and #29502) and for partnerships with the US Fish & Wildlife Service and the Friends of the Dunes. Patrick Hesp acknowledges Louisiana State University and Flinders University for support. Andrea Pickart and Patrick Hesp thank the USFWS Region 8 Inventory and Monitoring Program (award no. #F11PX02819 and #F14PX02390) and the Arcata Fish and Wildlife Office Coastal Program for funding and/or support in establishment and monitoring of beach dune transects reported in this study.

All authors would like to thank Dr. Conor Shea for substantial contributions to transect monitoring and expertise in RTK GIS and data processing. We also thank Graziela Miot da Silva for support with wind data calculations. Additional field support was provided by Laurel Goldsmith, Desiree Davenport, Britney Newby, Ashley Dickinson, Kelsey McDonald, Michael Grilliot, and Derek Heathfield.

References

Abeysirigunawarbena, D.S., Walker, I.J., 2008. Sea level responses to climate variability and change in northern British Columbia. Atmosphere-Ocean 46 (3), 277–296.

Abeysirigunawarbena, D.S., Gilleland, E., Bronaugh, D., Wong, P., 2009. Extreme wind regime responses to climate variability and change in the inner south coast of British Columbia. Canada. Atmosphere-Ocean 47 (1), 1480–9214.

Abhar, K.C., Walker, I.J., Hesp, P.A., Gares, P., 2015. Spatial-temporal evolution of aeolian blowout dunes at Cape Cod. Geomorphology 236, 148–162.

Allan, J.C., Komar, P.D., 2002. Extreme storms on the Pacific Northwest coast during the 1997–98 El Niño and 1998–99 La Niña. J. Coast. Res. 18 (1), 175–193.

Allan, J.C., Komar, P.D., Priest, G.R., 2003. Shoreline variability on the high-energy Oregon Coast and its usefulness in erosion-hazard assessments. J. Coast. Res. 38 (183-105). Andrews, B.D., Gares, P.A., Colby, J.D., 2002. Techniques for GIS modeling of coastal dunes.

Geomorphology 48, 289–308.

Anthony, E.J., Vanhee, S., Ruz, M., 2006. Short-term beach-dune sand budgets on the North Sea coast of France: sand supply from shoreface to dunes, and the role of wind and fetch. Geomorphology 81 (3–4), 316–329.

Arens, S.M., 1996. Patterns of sand transport on vegetated foredunes. Geomorphology 17, 339–350

Arens, S.M., Wiersma, J., 1994. The Dutch foredunes: inventory and classification. J. Coast. Res. 10 (1), 189–202.

Arens, S., Slings, Q., Geelen, L., 2013. Restoration of dune mobility in the Netherlands. In:
Martinez, M.L., Delgado-Fernandez, J.B., Hesp, P.A. (Eds.), Restoration of Coastal Dunes.
Springer Series on Environmental Management. Springer-Verlag, Berlin, pp. 107–124.

Bagnold, R.A., 1941. The Physics of Blown Sand and Desert Dunes. Methuen, London. Barnard, P., Short, A., Harley, M., Splinter, K., Vitousek, S., Turner, I., Allan, J., Banno, M., Bryan, K., Doria, A., Hansen, J., Kato, S., Kuriyama, Y., Randall-Goodwin, E., Ruggiero, P., Walker, I.J., Heathfield, D., 2015. Coastal vulnerability across the Pacific dominated

by El Niño/Southern Oscillation. Nat. Geosci. 8, 801–807.

Barnard, P.L., Hoover, D., Hubbard, D.M., Snyder, A., Ludka, B.C., Allan, J., Kaminsky, G.M., Ruggiero, P., Gallien, T.W., Gabel, L., McCandless, D., Weiner, H.M., Cohn, N., Anderson, D.L., Serafin, K.A., 2017. Extreme oceanographic forcing and coastal response due to the 2015–2016 El Nino. Nat. Commun. 8. https://doi.org/10.1038/ncomms14365.

Bauer, B.O., Davidson-arnott, R.G.D., 2002. A general framework for modelling sediment supply to coastal dunes including wind angle, beach geometry, and fetch effects. Geomorphology 49, 89–108.

Blott, S.J., Pye, K., 2001. GRADISTAT: a grain size distribution and statistics package for the analysis of unconsolidated sediments. Earth Surf. Process. Landf. 26, 1237–1248.

Cooper, W.S., 1967. Coastal dunes of California. Geol. Soc. Am. Mem. 104, 1–147.
Darke, I.B., Eamer, J.B.R., Beaugrand, H.E.R., Walker, I.J., 2013. Monitoring considerations for a dynamic dune restoration project: Pacific Rim National Park Reserve, British Columbia, Canada. Earth Surf. Process. Landf. 38 (9), 983–993.

Darke, I.B., Walker, I.J., Hesp, P.A., 2016. Beach-dune sediment budgets and dune morphodynamics following coastal dune restoration, Wickanninish Dunes, Canada. Earth Surf. Process, Landf. 41 (10), 1370–1385.

Davidson-Arnott, R.G.D., 2010. Introduction to Coastal Processes and Geomorphology. Cambridge University Press, New York, NY.

Davidson-Arnott, R.G.D., Law, M.N., 1996. Measurement and prediction of long-term sediment supply to coastal foredunes. J. Coast. Res. 12 (3), 654–663.

Davies, K.W., Petersen, S.L., Johnson, D.D., Davis, D.B., Madsen, M.D., Zvirzdin, D.L., Bates, J.D., 2010. Estimating juniper cover from National Agriculture Imagery Program (NAIP) imagery and evaluating relationships between potential cover and environmental variables. Rangel. Ecol. Manag. 63, 630–637.

De Vries, S., Southgate, H.N., Kanning, W., Ranasinghe, R., 2012. Dune behaviour and aeolian transport on decadal timescales. Coast. Eng. 67, 41–53.

Delgado-Fernandez, I., Davidson-Arnott, R., 2009. Sediment input to foredunes: description and frequency of transport events at Greenwich Dunes, PEI, Canada. J. Coast. Res. SI56, 302–306.

Delgado-Fernandez, I., Davidson-Arnott, R., 2011. Meso-scale aeolian sediment input to coastal dunes: the nature of aeolian transport events. Geomorphology 126 (1–2), 217–232.

Dingler, J.R., Clifton, H.E., 1994. Barrier systems of California, Oregon, and Washington. In: Davis, R.A. (Ed.), Geology of Holocene Barrier Island Systems. Springer-Verlag, New York, NY, pp. 115–166.

- Eamer, J.B.R., Walker, I.J., 2010. Quantifying sand storage capacity of large woody debris on beaches using LiDAR. Geomorphology 118, 33–47.
- Eamer, J.B.R., Walker, I.J., 2013. Quantifying spatial and temporal trends in beach-dune volumetric changes using spatial statistics. Geomorphology 191:94–108. https://doi. org/10.1016/j.geomorph.2013.03.005.
- Engelhart, S.E., Vacchi, M., Horton, B.P., Nelson, A.R., Kopp, R.E., 2015. A sea level database for the Pacific coast of central North America. Quat. Sci. Rev. 113, 78–92.
- Fisher, R.A., 1935. The Design of Experiments. Oliver & Boyd, London.
- Fryberger, S.G., Dean, G., 1979. Dune forms and wind regime. In: McKee, E.D. (Ed.), A Study of Global Sand Seas, Geol. Survey prof. Paper 1052. 1979. US Govt. Printing Office, Washington, pp. 137–170.
- Gares, P.A., Nordstrom, K.F., 1995. A cyclic model of foredune blowout evolution for a leeward coast: Island Beach, New Jersey. Ann. Assoc. Am. Geogr. 85 (1), 1–20.
- Godfrey, P.J., 1977. Climate, plant response, and development of dunes on barrier beaches along the US east coast. Int. J. Biometeorol. 21, 203–215.
- Goldsmith, V., 1989. Coastal sand dunes as geomorphological systems. Proc. R. Soc. Edinb. B 96B 3–15
- Hapke, C.J., Reid, D., Richmond, B.M., Ruggiero, P., List, J., 2006. National Assessment of Shoreline Change Part 3: Historical Shoreline Change and Associated Coastal Land Loss Along Sandy Shorelines of the California Coast. Open-file Report 2006. p. 1219.
- Hapke, C.J., Reid, D., Richmond, B., 2009. Rates and trends of coastal change in California and the regional behaviour of the beach and cliff system. J. Coast. Res. 25 (3), 603–615
- Harris, C.K., Traykovski, P.A., Geyer, W.R., 2005. Flood dispersion and deposition by near-bed gravitational sediment flows and oceanographic transport: a numerical modeling study of the Eel River shelf, northern California. J. Geophys. Res. 110 (C9). https://doi.org/ 10.1029/2004IC002727.
- Heathfield, D.K., Walker, I.J., 2011. Analysis of coastal dune dynamics, shoreline position, and large woody debris at Wickaninnish Bay, Pacific Rim National Park, British Columbia. Can. J. Earth Sci. 48 (7), 1185–1198.
- Heathfield, D.K., Walker, I.J., Atkinson, D.E., 2013. Erosive water level regime and climatic variability forcing of beach-dune systems on south-western Vancouver Island, British Columbia, Canada. Earth Surf. Process. Landf. 38 (7), 751–762.
- Hemming, M.A., Nieuwenhuize, J., 1990. Seagrass wrack-induced dune formation on a tropical coast (Banc d'Arguin, Mauritania). Estuar. Coast. Shelf Sci. 31, 499–502.
- Hesp, P.A., 1984. Foredune formation in Southeast Australia. In: Thom, B.G. (Ed.), Coastal Geomorphology in Australia. Academic Press, pp. 69–97.
- Hesp, P.A., 1988a. Morphology, dynamics and internal stratification of some established foredunes in Southeast Australia. Sediment. Geol. 55 (1–2), 17–41.
- Hesp, P.A., 1988b. Surfzone, beach and foredune interactions on the Australian southeast coast. J. Coast. Res. 3, 15–25.
- Hesp, P.A., 1989. A review of biological and geomorphological processes involved in the initiation and development of incipient foredunes. Proc. R. Soc. Edinb. B 98B,
- Hesp, P., 2002. Foredunes and blowouts: initiation, geomorphology and dynamics. Geomorphology 48 (1–3), 245–268.
- Hesp, P., 2013. A 34 year record of foredune evolution, Dark Point, NSW, Australia. J. Coast. Res. 65 (sp2), 1295–1300.
- Hesp, P.A., Smyth, T.A.G., 2016. Surfzone-beach-dune interactions: review and the role of the intertidal beach. J. Coast. Res. (S.I. 75), 8–12.
- Houser, C., 2012. Feedback between ridge and swale bathymetry and barrier island storm response and transgression. Geomorphology 173–174, 1–16.
- Houser, C., Ellis, J., 2013. Beach and Dune Interaction. Treatise on Geomorphology. vol. 10. Elsevier Ltd.. https://doi.org/10.1016/B978-0-12-374739-6.00283-9.
- Houser, C., Hapke, C., Hamilton, S., 2008. Controls on coastal dune morphology, shoreline erosion and barrier island response to extreme storms. Geomorphology 100 (3–4), 223–240.
- Jungerius, P.D., van der Meulen, F., 1989. The development of dune blowouts as measured with erosion pins and sequential air photos. Catena 16, 369–376.
- Kuriyama, Y., Mockizuki, N., Nakashima, T., 2005. Influence on vegetation on aeolian sand transport from a backshore to a foredune in Hasaki, Japan. Sedimentology 52, 1123–1132.
- Luna, M.C.M., Parteli, E.J.R., Duran, O., Herrmann, H.J., 2011. Model for the genesis of coastal dune fields with vegetation. Geomorphology 129, 215–224.
- McLean, R.F., Thom, B.G., 1975. Beach changes at Moruya, 1974–74. Second Australian Conference on Coastal and Ocean Engineering, 1975: The Engineer, the Coast and the Ocean. Institution of Engineers, Sydney, Australia, pp. 12–17.
- Miot da Silva, G., Hesp, P., 2010. Coastline orientation, Aeolian sediment transport and foredune and dunefield dynamics of Mocambique Beach, Southern Brazil. Geomorphology 120 (3), 258–278.
- Nordstrom, K.F., Jackson, N.L., Korotky, K.H., 2011a. Aeolian sediment transport across beach wrack. J. Coast. Res. (SI59), 211–217.
- Nordstrom, K.F., Jackson, N.L., Korotky, K.H., Puleo, J.A., 2011b. Aeolian transport rates across raked and unraked beaches on a developed coast. Earth Surf. Process. Landf. 36, 779–789.
- Ollerhead, J., Davidson-Arnott, R., Walker, I.J., Mathew, S., 2013. Annual to decadal morphodynamics of the foredune system at Greenwich Dunes, Prince Edward Island, Canada. Earth Surf. Process. Landf. 38 (3), 284–298.

- Patsch, K., Griggs, G., 2006. Littoral Cells, Sand Budgets, and Beaches: Understanding California's Shoreline. Institute of Marine Sciences, University of California, Santa Cruz.
- Pickart, A.J., 2013. Dune restoration over two decades at the Lanphere and Ma-le'l Dunes in northern California. In: Martinez, M.L., et al. (Eds.), Restoration of Coastal Dunes. Springer, Berlin, Heidelberg, pp. 159–171.
- Pickart, A., 2014. Predicting and Measuring Climate Change Impacts at a Coastal Dune Site: A Progress Report. USFWS Pub. Arcata, CA.
- Pickart, A.J., Barbour, M.G., 2007. Beach and dune. In: Barbour, M.G., Keeler-Wolf, T., Schoenherr, A.A. (Eds.), Terrestrial Vegetation of California. University of California Press, Los Angeles, CA.
- Pickart, A.J., Sawyer, J.O., 1998. Ecology and Restoration of Northern California Coastal Dunes. California Native Plant Society, Sacramento, CA.
- Psuty, N.P., 1988. Sediment budget and dune/beach interaction. J. Coast. Res. Spec. Issue 3,
- Ruggiero, P., Komar, P.D., McDougal, W.G., Marra, J.J., Beach, R.A., 2001. Wave runup, extreme water levels and the erosion of properties backing beaches. J. Coast. Res. 17 (2) 407–419
- Ruggiero, P., Buijsman, M., Kaminsky, G.M., Gelfendbaum, G., 2010. Modeling the effects of wave climate and sediment supply variability on large-scale shoreline change. Mar. Geol. 273 (1–4), 127–140.
- Ruggiero, P., Mull, J., Zarnetske, P., Hacker, S., Seabloom, E., 2011. Interannual to decadal foredune evolution. Proc. Coast. Sediment. 2011 (3), 698–711.
- Runyan, K., Griggs, G.B., 2003. The effects of armouring seacliffs on the natural sand supply to the beaches of California. J. Coast. Res. 19 (2), 336–347.
- Sallenger Jr, A.H., Krabill, W., Brock, J., Swift, R., Manizade, S., Stockdon, H., 2002. Sea-cliff erosion as a function of beach changes and extreme wave runup during the 1997– 1998 El Niño. Mar. Geol. 187 (3-4), 279–297.
- Sawyer, J.O., Keeler-Wolf, T., Evens, J.M., 2009. A Manual of California Vegetation. California Native Plant Society, Sacramento, CA.
- Schwing, F.B., Murphree, T., Green, P.M., 2002. The northern oscillation index (NOI): a new climate index from the northeast Pacific. Prog. Oceanogr. 53 (2–4), 115–139.
- Scott, D., Mathew, S., Davidson-Arnott, G.D., Ollerhead, J., 2010. Evolution of a beach-dune system following a catastrophic storm overwash event: Greenwich Dunes, Prince Edward Island, 1936–2005. Can. J. Earth Sci. 47 (3), 273–290.
- Sherman, D.J., Bauer, B.O., 1993. Dynamics of beach-dune systems. Prog. Phys. Geogr. 17 (4), 413–447.
- Short, A.D., Hesp, P.A., 1982. Wave, beach and dune interactions in southeastern Australia. Mar. Geol. 48 (3–4), 259–284.
- Storlazzi, C.D., Griggs, G.B., 2000. Influence of El Nino-Southern Oscillation (ENSO) envents on the evolution of central California's shoreline. GSA Bull. 112 (2), 236–249.
- Storlazzi, C.D., Wingfield, D.K., 2005. Spatial and Temporal Variations in Oceanographic and Meteorologic Forcing Along the Central California Coast, 1980–2002. Open File Report, 2005. p. 5085.
- Storlazzi, C.D., Willis, C.M., Griggs, G.B., 2000. Comparative impacts of the 1982–83 and 1997–98 El Niño winters on the central California coast. J. Coast. Res. 16 (4), 1022–1036
- Subbotina, M.M., Thomson, R.E., Rabinovich, A.B., 2001. Spectral characteristics of sea level variability along the west coast of North America during the 1982–83 and 1997–98 El Niño events. Prog. Oceanogr. 49 (1–4), 353–372.
- Thieler, E.R., Danforth, W.W., 1994. Historical shoreline mapping (II): application of the digital shoreline mapping and analysis systems (DSMS/DSAS) to shoreline change mapping in Puerto Rico. J. Coast. Res. 10 (3), 600–620.
- Thieler, E.R., Himmelstoss, E.A., Zichichi, J.L., Ergul, Ayhan, 2009. Digital Shoreline Analysis System (DSAS) Version 4.0—An ArcGIS Extension for Calculating Shoreline Change: U.S. Geological Survey Open-file Report 2008-1278.
- Walker, I.J., Davidson-Arnott, R.G.D., Bauer, B.O., Hesp, P.A., Delgado-Fernandez, I., Ollerhead, J., Smyth, T.A.J., 2017. Scale dependent perspectives on the geomorphology and evolution of beach-dune systems. Earth Sci. Rev. 171, 220–253.
- Wang, J., Ge, Y., Heuvelink, G.B.M., Zhou, C., Brus, D., 2012. Effect of sampling design on ground control points on the geometric correction of remotely sensed imagery. Int. J. Appl. Earth Obs. Geoinf. 18, 91–100.
- Warrick, J.A., 2014. Eel River margin source-to-sink sediment budgets: revisited. Mar. Geol. 351, 25–37.
- Wheatcroft, R.A., Sommerfield, C.K., 2005. River sediment flux and shelf accumulation rates on the Pacific Northwest margin. Cont. Shelf Res. 25, 311–332.
- Williams, T., Patton, J.R., Sutherland, D., 2013. Tectonic Land Level Changes & Their Contributions to Sea-level Rise, Humblodt Bay Region, Northern California. Cascadia Geosciences Report: F11AC01092.
- Willis, C.M., Griggs, G.B., 2003. Reduction in fluvial sediment discharge by coastal dams in California and implications for beach sustainability. J. Geol. 111 (2), 167–182.
- Wolter, K., Timlin, M.S., 1998. Measuring the strength of ENSO events: how does 1997/98 rank? Weather 53 (9), 315–324.